

CANADIAN THESES ON MICROFICHE

I.S.B.N.

THESES CANADIENNES SUR MICROFICHE



National Library of Canada
Collections Development Branch

Canadian Theses on
Microfiche Service

Ottawa, Canada
K1A 0N4

Bibliothèque nationale du Canada
Direction du développement des collections

Service des thèses canadiennes
sur microfiche

NOTICE

The quality of this microfiche is heavily dependent upon the quality of the original thesis submitted for microfilming. Every effort has been made to ensure the highest quality of reproduction possible.

If pages are missing, contact the university which granted the degree.

Some pages may have indistinct print, especially if the original pages were typed with a poor typewriter ribbon or if the university sent us a poor photocopy.

Previously copyrighted materials (journal articles, published tests, etc.) are not filmed.

Reproduction in full or in part of this film is governed by the Canadian Copyright Act, R.S.C. 1970, c. C-30. Please read the authorization forms which accompany this thesis.

**THIS DISSERTATION
HAS BEEN MICROFILMED
EXACTLY AS RECEIVED**

AVIS

La qualité de cette microfiche dépend grandement de la qualité de la thèse soumise au microfilmage. Nous avons tout fait pour assurer une qualité supérieure de reproduction.

S'il manque des pages, veuillez communiquer avec l'université qui a conféré le grade.

La qualité d'impression de certaines pages peut laisser à désirer, surtout si les pages originales ont été dactylographiées à l'aide d'un ruban usé ou si l'université nous a fait parvenir une photocopie de mauvaise qualité.

Les documents qui font déjà l'objet d'un droit d'auteur (articles de revue, examens publiés, etc.) ne sont pas microfilmés.

La reproduction, même partielle, de ce microfilm est soumise à la Loi canadienne sur le droit d'auteur, SRC 1970, c. C-30. Veuillez prendre connaissance des formules d'autorisation qui accompagnent cette thèse.

**LA THÈSE A ÉTÉ
MICROFILMÉE TELLE QUE
NOUS L'AVONS REÇUE**

National Library
of CanadaBibliothèque nationale
du Canada

Canadian Theses Division / Division des thèses canadiennes

Ottawa, Canada
K1A 0N4

56889

PERMISSION TO MICROFILM — AUTORISATION DE MICROFILMER

• Please print or type — Écrire en lettres mouées ou dactylographier

Full Name of Author — Nom complet de l'auteur

JOHN WAYNE LOGUS

Date of Birth — Date de naissance

24/05/51

Country of Birth — Lieu de naissance

CANADA

Permanent Address — Résidence fixe

5114-36 ST
RED DEER
ALTA

T4N 0T2

Title of Thesis — Titre de la thèse

Single Photon Emission Computed Tomography in Analysis of
Deposition and Distribution of 1.µm Particles in the
Normal Human Lung

University — Université

U of A

Degree for which thesis was presented — Grade pour lequel cette thèse fut présentée

M Sc

Year this degree conferred — Année d'obtention de ce grade

1982

Name of Supervisor — Nom du directeur de thèse

SFP MAN

Permission is hereby granted to the NATIONAL LIBRARY OF
CANADA to microfilm this thesis and to lend or sell copies of
the film.The author reserves other publication rights, and neither the
thesis nor extensive extracts from it may be printed or other-
wise reproduced without the author's written permission.L'autorisation est, par la présente, accordée à la BIBLIOTHÈ-
QUE NATIONALE DU CANADA de microfilmer cette thèse et de
prêter ou de vendre des exemplaires du film.L'auteur se réserve les autres droits de publication; ni la thèse
ni de longs extraits de celle-ci ne doivent être imprimés ou
autrement reproduits sans l'autorisation écrite de l'auteur.

Date

April 21/82

Signature

Wayne Logus

THE UNIVERSITY OF ALBERTA

SINGLE PHOTON EMISSION COMPUTED TOMOGRAPHY IN
ANALYSIS OF DEPOSITION AND DISTRIBUTION OF 1 μ m
PARTICLES IN THE NORMAL HUMAN LUNG

by



J. WAYNE LOGUS

A THESIS

SUBMITTED TO THE FACULTY OF GRADUATE STUDIES

AND RESEARCH IN PARTIAL FULFILMENT OF THE

REQUIREMENTS FOR THE DEGREE OF

MASTER OF SCIENCE

IN

EXPERIMENTAL MEDICINE

DEPARTMENT OF MEDICINE

EDMONTON, ALBERTA

SPRING, 1982

THE UNIVERSITY OF ALBERTA

RELEASE FORM

NAME OF AUTHOR - J. Wayne Logus

TITLE OF THESIS - Single Photon Emission Computed Tomography
in Analysis of Deposition and Distribution
of 1 μ m Particles in the Normal Human Lung

DEGREE FOR WHICH THESIS WAS PRESENTED - MSc

YEAR THIS DEGREE GRANTED - 1982

Permission is hereby granted to THE UNIVERSITY OF ALBERTA LIBRARY to reproduce single copies of this thesis and to lend or sell such copies for private, scholarly or scientific research purposes only.

The author reserves other publication rights, and neither the thesis nor extensive extracts from it may be printed or otherwise reproduced without the author's written permission.

J. Wayne Logus.....

PERMANENT ADDRESS

5114-36 Street

Red Deer, AB

T4N 0T2

DATED April 1, 1982

THE UNIVERSITY OF ALBERTA
FACULTY OF GRADUATE STUDIES AND RESEARCH

The undersigned certify that they have read, and recommend to the Faculty of Graduate Studies and Research, for acceptance, a thesis entitled Single Photon Emission Computed Tomography in Analysis of Deposition and Distribution of 1 μ m Particles in the Normal Human Lung submitted by J. Wayne Loqus in partial fulfilment of the requirements for the degree of Master of Science in Experimental Medicine.

.....
Supervisor
.....
.....
.....

Date April 1, 1982

To Lissie

ABSTRACT

In the past, the study of radiolabeled aerosols in humans has been carried out using probes, rectilinear scanners, or conventional gamma cameras. We have applied single photon emission computed tomography (SPECT) to provide 3-dimensional analysis of particle deposition. A DeVilbiss 40 nebulizer was used to generate an aerosol of ^{99m}Tc sulfur colloid, and a reservoir bag (8 l) was interposed between the subject and the aerosol generator. The activity median aerodynamic diameter of the particle as sized with an Andersen Cascade impactor was 1.2 μm and the associated geometric standard deviation was 1.8.

The subjects were scanned in the supine position by a GE 400T gamma camera system. Image reconstruction was carried out on a PDP 11/70 computer simultaneously with data acquisition. Image display and analysis were carried out on a PDP 11/34 operating on the GAMMA-11 system and with special user written programmes.

Subjects typically received 35 MBq of activity which corresponded to a maximum lung dose of 4.5 mGy. Scan time was 40 minutes. The tomographic reconstruction consisted of 192 frames which provided coronal, axial and sagittal planes of the lung image. Slice thickness was 6 mm. Tomography allowed us to obtain regional count information at any depth within the lung independent of the surrounding regions. Accordingly, the conventional xenon imaging was not required to determine regional lung volumes.

Thirteen normal subjects were studied in two series. In the first series we found a significantly higher deposition of aerosol in the apical and posterior basal segments of the lower lobes in both lungs than elsewhere. From the second experimental series we determined that this was due, at least in part, to the positioning of the arms by the side. Analysis of perfusion obtained with the subjects receiving the injection of ^{99m}Tc -MAA in the sitting position also showed higher perfusion in the apical and posterior basal segments of the lower lobes. These findings illustrate the similarity in the distribution of both aerosol deposition and perfusion.

We conclude that SPECT will prove to be a useful addition to the study of particle deposition in man, provided that care is taken to avoid the reconstruction artifacts caused by the arms and an appropriate form of attenuation correction is incorporated into the reconstruction programme.

ACKNOWLEDGMENTS

I would like to express my sincere gratitude to my supervisor, Dr. Paul Man for his continued guidance, and encouragement throughout this project. The assistance of my advisors, Dr. Brian Lentle, Dr. Tony Noujaim, and Dr. Brian Sproule is also gratefully acknowledged.

Special thanks to Dr. Rick Hooper for the hours he spent developing the computer programmes which made the whole project possible, and also for the time he spent in explaining the theory and technique behind the computer and gamma camera systems.

I would also like to acknowledge the assistance of the staff of the Nuclear Medicine Department of the Cross Cancer Clinic, the staff of the Pulmonary Function Laboratory at the University Hospital, to John Scott and his co-workers at the Edmonton Radiopharmaceutical Center, and to King Mok for his excellent technical assistance.

Financial support from the Alberta Heritage Foundation for Medical Research in the form of equipment grants, studentships, and research allowances and from the University of Alberta in the form of a Graduate Assistantship are gratefully acknowledged.

TABLE OF CONTENTS

CHAPTER	PAGE
I THE PROBLEM	1
i) BACKGROUND TO THE PROBLEM	2
ii) STATEMENT OF THE PROBLEM	3
iii) RESEARCH HYPOTHESIS	4
iv) OBJECTIVES AND RESEARCH LIMITATIONS	4
II LITERATURE SURVEY	5
i) INTRODUCTION	6
ii) GENERAL PROPERTIES OF AN AEROSOL	7
-Electrical Charge	8
iii) AEROSOL GENERATION	11
-Monodispersed	11
-Polydispersed	14
iv) PARTICLE SIZING	20
-Introduction	20
-Cascade Impactors	25
-The Effect of Ionic Concentration on the Size of Aqueous Aerosols	27
v) PARTICLE DEPOSITION	31
-Mechanics of Deposition	31
-Regional Deposition	35
-Total Deposition of Particles in the Lung	38
-Particle Clearance	41
-Regional Distribution Variations in Aerosol Deposition	43

vi)	GAMMA CAMERA EMISSION TOMOGRAPHY	47
III	EXPERIMENTAL	50
i)	PARTICLE GENERATION AND SIZING	51
ii)	CALIBRATION OF THE CASCADE IMPACTOR	57
iii)	PHANTOM MEASUREMENTS	59
	-Introduction	59
	-Resolution Measurements	60
	-Comparison of Regional Count Densities and the Effects of Attenuation	63
iv)	METHOD AND DESCRIPTION FOR THE HUMAN TRIAL	68
v)	AEROSOL ADMINISTRATION	69
vi)	RADIOACTIVE LUNG BURDEN DUE TO AEROSOL ADMINISTRATION	71
vii)	QUALITY CONTROL IN THE RADIOGOLLOID PREPARATIONS	73
viii)	LUNG IMAGING AND TOMOGRAPHIC RECONSTRUCTION	75
ix)	DATA ANALYSIS AND RESULTS IN THE HUMAN TRIAL SERIES 1	76
x)	DATA ANALYSIS AND RESULTS IN THE HUMAN TRIAL SERIES 2	86
xi)	A COMPARISON BETWEEN REGIONAL BLOOD PERFUSION AND AEROSOL DEPOSITION	88

IV	DISCUSSION	91
	i) PHANTOM MEASUREMENTS	92
	ii) THE HUMAN TRIAL	95
	-Series 1, Sagittal Analysis	96
	-Anterior-Posterior ROI Comparison	98
V	CONCLUSION	104

* * *

REFERENCES	109
GENERAL BIBLIOGRAPHY	117
APPENDIX 1 TABLE XI	128
APPENDIX 2 TABLE XII	129
APPENDIX 3 TABLE XIII	130
APPENDIX 4 TABLES XIV, XV, AND XVI	134
APPENDIX 5 TABLE XVII	136
APPENDIX 6 TABLE XVIII	137
APPENDIX 7 TABLE XIX	138

LIST OF TABLES

TABLE	DESCRIPTION	PAGE
I	Operating and output characteristics of the DeVilbiss nebulizer (vent closed)	17
II	Calculation of evaporation times of isolated water droplets in air of different humidities at 21 C° and 760 mm pressure.	27
III	Per cent supersaturation of the atmosphere required to hold, in equilibrium, isolated water droplets of various sizes.	28
IV	Sizes of the spherical "lesions" in the glass phantom.	60
V	Resolution of the spheres within the phantom at various sphere to background ratios.	62
VI	Count density data through the cold 20 mm sphere taken from the reconstructed phantom scan.	63

VII	The distribution of activity in a defined quadrant of the lung expressed as a percentage of total activity.	77
VIII	Counts (arbitrary units) of anterior and posterior ROI from axial frames of subject MY.	80
IX	Levels of significance between anterior and posterior ROI in the lower areas of the lung.	82
X	A comparison of the distribution of ^{99m}Tc MAA (Perfusion) and ^{99m}Tc sulphur colloid aerosol in the right lung of subject LO.	89

APPENDIX

XI	Summary of the aerosol sizing trials carried out with the Bendix ultrasonic nebulizer.	128
XII	Summary of the aerosol sizing trials carried out with an Airlife and Hudson nebulizers.	129
XIII	Summary of the aerosol sizing trials carried out with the DeVilbiss nebulizer.	130

XIV	Horizontal (X axis) profile taken through the summed axial frames of the phantom.	134
XV	Vertical (Z axis) profile taken through the summed axial frames of the phantom.	134
XVI	Vertical (Y axis) profile taken through the summed coronal frames of the phantom.	135
XVII	Count densities from the anterior and posterior ROI located on axial planes of the phantom.	136
XVIII	Pulmonary function data (% if predicted) for normal subjects.	137
XIX	Vertical profiles taken through static, sitting, anterior and posterior views of the right lung after aerosol inhalation on subject JH.	138

LIST OF FIGURES

Figure	Page
1. Diagram of the DeVilbiss model 40 nebulizer	15
2. Output and mass median diameter as functions of jet flow rate for the DeVilbiss 40 nebulizer.	17
3. A lognormal plot of a particle size distribution	22
4. An example of the lognormal distribution function in generalized linear form for $dg = 1.0$ and $\sigma g = 2.0$.	24
5. Size distribution plotted on lognormal probability paper for $dg = 1.0$ and $\sigma g = 2.0$.	24
6. Deposition fraction in each of the nasopharynx, tracheobronchial, and pulmonary regions of the lung for a given MMAD when σg varies from 1.2 to 4.5 and tidal volume is 1450 ml.	36
7. Theoretical prediction of deposition profile along the respiratory tract at 500 cm ³ tidal volume and 4-second breathing period for various particle diameters.	38

8. 6 l glass phantom with hollow spheres. 60

9. Schematic of the aerosol delivery system. 69

LIST OF PHOTOGRAPHIC PLATES

PLATE	DESCRIPTION	PAGE
1.	Horizontal slice (SH3) through summed axial slices of phantom showing typical "hammock" shape due to attenuation.	64
2.	Vertical slice (SV3) through summed axial slices of phantom showing typical "hammock" shape due to attenuation.	64
3.	Division of the left lung of subject JH into quadrants to illustrate regional count variations.	77
4.	Positions of the ROI in the lower (left) and upper (right) sections of axial slices of the lung.	79
5.	Count distribution through an axial slice (dual frame) of the lower right lung of the subject DJ to show regional variations.	83
6.	Vertical slice profile through the right static anterior (top) and posterior (bottom) lung images of the subject JH to show distribution variations.	102

GLOSSARY

Activity - A measurable property of a particulate population; e.g., mass, number, radioactivity, surface area.

Aerodynamic diameter - For any particle, the diameter of a sphere of unit density that has the same terminal settling velocity as the particle.

Aerosol - A suspension of solid or liquid particles in air.

Activity Median Aerodynamic Diameter (AMAD) - Fifty percent of airborne activity is associated with particles having aerodynamic diameters smaller than the AMAD.

Atomizer - A device with which droplets are produced by mechanical disruption of a bulk liquid.

Cascade impactor - An instrument consisting of a series of impaction stages of increasing efficiency with which particles can be segregated into relatively narrow intervals of aerodynamic diameters.

Coagulation - The collision and adherence of two particles to form a single larger particle.

Corona - A region of intense ionization formed in air about an electrode of small diameter when a sufficiently high voltage is applied to it.

Diffusion - The net movement of particles due to Brownian motion when a concentration gradient exists.

Elutriation - The separation of particles according to aerodynamic diameter by allowing them to settle through a moving air stream.

Geometric standard deviation - A measure of dispersion in a lognormal distribution.

Hatch-Choate Equations - Expressions relating the parameters of one lognormal activity distribution to those of another form of activity for the same population of particles.

Impaction - The process in which the inertia of particles in an air stream that is deflected about an obstacle causes them to strike the obstacle.

Lognormal distribution - A particle size distribution in which activity is normally distributed with respect to the logarithms of particle diameters.

Median diameter - A distribution parameter such that half of the particulate activity is associated with particles of smaller size.

Monodispersed - Having a small range of diameters ($\sigma_g < 1.2$)

Nebulizer - An atomizer that operates within a small container from which only a fraction of the droplets escape.

Particle size distribution - A mathematical relationship expressing the relative amount of activity associated with particles in a given element of size.

Photospectrometer - An instrument for measuring the diameter of a particle in terms of the amount of light it scatters into a fixed solid angle.

Polydispersed (heterodispersed) - Including a range of diameters ($\sigma_g \geq 1.2$).

Rebound - Return of particles to an air stream when they fail to adhere after striking a collecting surface.

Re-entrainment - Return of particles to an air stream some time after their deposition on a collecting surface.

Respirable activity - The fraction of airborne activity that will be deposited, according to one or another lung model, in the pulmonary compartment.

Sedimentation - movement of particles in the direction of the earth's center brought about by the force of gravity.

Sinclair-LaMer generator - A device for producing monodispersed aerosols by the controlled condensation of a vapor onto nuclei.

Slip factor - A correction to Stokes law made necessary by the existence of a finite net gas velocity at a particle surface.

Spinning disk (top) atomizer - A device with which monodispersed droplets are produced when a thin film of liquid breaks up on being thrown from the rim of a spinning disk.

Stokes diameter - For any particle, the diameter of a sphere having the same bulk density and same terminal settling velocity as the particle.

Stokes law - A relationship describing the force exerted by a viscous fluid of negligible inertia on a sphere moving at a constant velocity relative to the fluid.

Terminal settling velocity - The equilibrium velocity approached by a particle falling under the influence of gravity and fluid resistance.

Wall loss - The deposition of particles on sampler surfaces other than those designed to collect particles.

CHAPTER I

THE PROBLEM

BACKGROUND TO THE PROBLEM

The air we breathe is contaminated with smokes, dusts, allergens, micro-organisms, and other forms of toxic particles which cause a wide variety of pulmonary diseases. The concentration of these particles is much higher in urban centers (1,2) and with this increase, the likelihood of lung-related diseases also rises (3). It has been estimated that even non-polluted air may contain 10^9 particles / m^3 , and cities the size of Edmonton typically have dust concentrations averaging $125 \mu g/m^3$ of air (4).

The majority of pulmonary diseases, and many other non-pulmonary diseases in man enter the body through the respiratory system. The list includes tuberculosis, measles, influenza, one form of the plague, diphtheria, pneumococcal meningitis, and many others (5). The respiratory tract is also the most important route for the entry of toxic substances from occupational exposures. Some of the more important airborne particles which are known to produce occupational lung diseases are silicates, metals, respiratory carcinogens (arsenic, cobalt, asbestos, etc.), bacteria, fungi and viruses.

There are also positive aspects to the inhalation of aerosols. Clinically, aerosol mists are used in treating bronchospasm and allergies. By using pharmaceutical aerosols, it is possible to achieve high local concentrations of therapeutic agents directly in the airways without exposing the rest of the body to high systemic

concentrations.

Many investigators have attempted a wide variety of experiments with the goal of enhancing the understanding of the behavior of inhaled particles in the respiratory tract. Experiments have included the effects of particle size on regional deposition (6-20), the effects of the breathing pattern on particle deposition (21,22), and the relationship between deposition and lung anatomy (23,24).

STATEMENT OF THE PROBLEM

The conventional techniques for nuclear medicine imaging (gamma cameras or rectilinear scanners), are intrinsically limited in the information they provide in that they are displaying two-dimensional images of three-dimensional space. Accordingly, images from depth are superimposed on each other, resulting in a loss of resolution and detail, especially with respect to inhomogenous regions deep within the tissues being imaged.

In a manner analogous to the improvement of computer assisted tomography (CAT) over conventional X-rays, single photon emission computed tomography (SPECT) provides similar advantages to nuclear medicine imaging. The end result of both techniques is to improve the visual quality of the images obtained as well as to provide regional count density information through the incorporation of the 3-dimensional display.

RESEARCH HYPOTHESIS

The purpose of this study was to determine if single photon emission computed tomography could be of practical use in the investigation of regional deposition of small particles in the human lung.

OBJECTIVES AND RESEARCH LIMITATIONS

The study concentrated on the tomographic analysis of the deposition images obtained from the inhalation of ^{99m}Tc labelled sulphur colloid by a group of normal volunteers. Inhalation was carried out in the sitting position. The subjects were instructed on breathing patterns but there was no direct control over their inspiratory flow rates or tidal volumes. Aerosol generation and particle size remained unchanged throughout the series. In addition, the computer programme as written by Dr. Hooper remained basically unmodified and there was no attenuation corrections applied to the data during the tomographic reconstruction sequences.

CHAPTER II

LITERATURE SURVEY

INTRODUCTION

There are two basic purposes underlying pulmonary research into the behaviour of aerosols. First, to achieve a better understanding of the nature and behaviour of toxic airborne particles which may enter our respiratory tract during inhalation; and second, to gain information related to the site and extent of deposition of the medical sprays and mists used in the treatment of pulmonary disease.

In order to carry out any study involving aerosol deposition in the lung, a thorough understanding of the generation and behaviour of small particles is essential.

A summary of the properties of aerosols, aerosol generation, particle sizing and a resume of the research that has been carried out in the field of particle deposition in the lung is provided in the literature survey. Emphasis is placed on the material which is directly applicable to the experimental section of this thesis.

GENERAL PROPERTIES OF AN AEROSOL

In any study of aerosols, it is important to define as many of the particle parameters as possible. The complete list is extensive and includes such major factors as size and dispersion, shape, density, electrical charge, chemical composition, toxicity, and for liquid aerosols, the ionic concentration, viscosity, hygroscopic properties of the solute and relative humidity in the aerosol cloud.

In the field of pulmonary medicine the single most important parameter of an aerosol is the "size" of the particle. For a given study, an aerosol would ideally be monodispersed--that is, all particles would be of identical size. For practical purposes a quantitative definition was set forth by Fuchs and Sutugin (25) which considers an aerosol to be monodispersed if the coefficient of variation (standard deviation + mean diameter) is ≤ 0.2 , which is equivalent to a geometric standard deviation of 1.22 if the particle sizes follow a lognormal distribution.

The aerosol cloud can consist of either a pure solvent, a solute-solvent mixture (such as the bronchodilator medications), or solid particles.

A liquid droplet can also be used as a carrier for suspension of insoluble particles such as colloids.

A number of factors are constantly altering the mass and number of particles in an aerosol cloud. Particles are removed primarily by sedimentation, and to a lesser extent, electrostatic effects. For small particles, diffusion plays

an important role. In addition, coagulation within the cloud may lead to changes in the number, concentration, and particle size distributions. The operation of these factors will be examined in the following discussion.

Electrical Charge

Surface charges can be produced by the so-called triboelectric (26) effect when dry, non-metallic particles are generated into the air by such mechanisms as elutriation. The average number of charges per particle is related to particle diameter (27). This charge can affect inter-particle attractions and, depending on the medium surrounding the aerosol cloud, the rate of deposition and sedimentation of the particles. As sulphur colloid was used in the experiments to be described later, particular attention will be paid to the charge production phenomena of atomized colloid suspensions. When a droplet is formed by mechanical disruption of a body of conducting liquid, it may carry with it a net charge as a result of purely statistical fluctuation of positive and negative charges within the volume of the droplet.

The absolute value of excess charge has been shown by von Smoluchowski (28) for a spherical volume of diameter D (in μm) to be:

$$[\bar{q}] = 8.2 \times 10^{-7} \cdot D^{3/2} N^{1/2} \quad \text{Eq. (1)}$$

where N is the number of ions of one sign per cubic centimeter and $[\bar{q}]$ is a unit of electric charge (28).

The formula refers to the droplet volume while still in the bulk liquid and is related to the ionic concentration of the solution. Discharge can occur during the formation of the droplet as the ionic strength increases and this tends to reduce the charge as calculated by the equation. Natanson (29) found that up to an ionic concentration of approximately 10^{15} ions/cm³ there was essentially no discharge from the droplet during its formation. Increasing the ionic concentration above 10^{15} cm⁻³, the droplet charge per ion was found to diminish continuously to reach a plateau at about 10^{18} ions/cm³ at which point

$$[\bar{q}] = 5.6 D^{1/2} \quad \text{Eq. (2)}$$

where D is again in microns and $[\bar{q}]$ is the number of electric charges.

The induced charge can have several effects on the aerosol including altering apparent particle size and lowering the vapour pressure on the surface of the droplet. The most significant implication is, however, its effect in lung deposition. Despite the fact that theoretical and experimental evidence support the view that electric charge is ineffective after a particle has entered the respiratory tract, aerosol generation methods which produce charged particles consistently show greater overall

deposition than condensation methods which seldom yield charged particles, (30)

Suspensions of colloidal or insoluble particles may well have ionic concentrations in the region of maximum charging effect. In order to neutralize the charge on these aerosols, it is necessary to expose the aerosol to a very high bipolar concentration of ions. This can be achieved by using radioactive sources (31) or with a corona discharge in a suitably designed jet orifice. (32)

AEROSOL GENERATION

In order to gain a better understanding of airborne toxic particles, researchers have developed several methods of generating and monitoring aerosols which allow studies to be conducted on the mechanics of deposition and lung clearance. While it is desirable to conduct studies with monodispersed aerosols, the nature of many studies requires that the generated aerosols, to some degree, be polydispersed. The various systems available to produce either mono or polydispersed aerosols will be looked at briefly.

a) Monodispersed Aerosols

Condensation Aerosols

Probably the first apparatus available for producing aerosols with a narrow size range was done by a controlled condensation of organic vapors. Developed by Sinclair and LaMer (33), the system utilized a boiler, a reheater, and a cooling chimney. The boiler, containing the solution to be aerosolized, was maintained at some fixed temperature between 100 and 200°C. The reheater was kept at a temperature sufficient to vaporize all aerosol material which entered. Droplet nuclei were then produced by either an electric spark or by heating a wire coated with some inorganic salt. As the vapor is mixed with the nuclei in the condensation chimney, the particles are "grown" to the desired size by carefully controlling the cooling rate.

The first monodispersed aerosol used to study

deposition in the human respiratory tract was produced by the condensation of glycerol vapors on radioactive sodium chloride nuclei (34). The mean diameter of the different aerosols ranged from 0.4 to 5.8 μm with coefficients of variation less than 0.2.

Spinning Disk Atomizers

It was observed that droplets of uniform size are thrown from the rim of a spinning disk when a liquid is fed at a controlled rate onto the center of the disk. The liquid is spun off the edge of the disk when the centrifugal force overcomes the capillary force of the liquid. Walton and Prewett (35) found that most of the atomized liquid went into the formation of drops of the predicted diameter, but a small fraction of it appeared in the form of much smaller "satellite" droplets.

May (36) improved their system by extending its range of stable operation to 240,000 r.p.m., and providing a simple method to remove satellite droplets. He found that on the average there were four satellite droplets for each primary drop with the former having a diameter about one-fourth larger than the latter. The system is capable of generating liquid drops from 200 μm down to 10 μm which is near the useful limit of the apparatus (37). Further modification by Whitby et al (38), and Lippmann and Albert (39), have allowed production of dry particles having diameters between 1 and 10 μm .

A summary of the performance data on the various spinning disk generators is provided by Mercer (30).

Atomization of Suspensions of Monodispersed Particles

Monodispersed latex spheres such as those produced by Dow Chemical can be suspended in solution and nebulized using the ordinary air-blast nebulizer. If the aerosol produced is dried, the result will be an aerosol with the original size of the latex spheres. Care must be taken, however, to maintain a sufficiently low concentration of particles in order to avoid the production of too many liquid droplets containing 2 or more suspended particles which result in the production of multiple dry particles and accordingly increase the geometric standard deviation.

The probability (P) that droplets of a given size will contain x particles is given by the Poisson equation:

$$P(x) = m^x \cdot e^{-m}/x! \quad \text{Eq. (3)}$$

where $m = C_p \cdot V_s$ is the average number of individual particles expected in a droplet of volume V_s from a suspension containing C_p individual particles per unit volume.

Raabe (40) has derived an empirical calculation based on this equation which takes into consideration the fact that the droplet distribution from air-blast and ultrasonic nebulizers is polydispersed. His equation gives the

dilution factor Y , necessary to provide a desired singlet ratio R , which is the number of droplets containing single particles relative to the total number of droplets containing particles.

$$Y = f \cdot D^3_g \cdot \exp(4.5 \ln^2 \sigma_g) \cdot [1 - 0.5 \cdot \exp(\ln^2 \sigma_g)] / (1-R) D_i^3$$

Eq. (4)

where f is the volume fraction of individual particles of diameter D_i in the original suspension, D^3_g is the volume median diameter of the droplet distribution.

B) Polydispersed Aerosols

Air-blast Nebulizers

This method of nebulization is probably the most common system used to provide aerosols for studies of inhalation toxicity as well as the method of choice in self-administered medicinal mists. Figure 1 represents the DeVilbiss No. 40 glass nebulizer, (The DeVilbiss Company, Somerset, Pennsylvania), one of the simplest and most widely used devices of this sort.

A venturi effect at the mouth of the liquid inlet tube produces a drop in pressure at that point and causes a flow of liquid up the inlet tube and into the air stream. The jet of air entrains a filament of liquid, drawing it out to some unstable length at which point it breaks up to form droplets of various sizes.

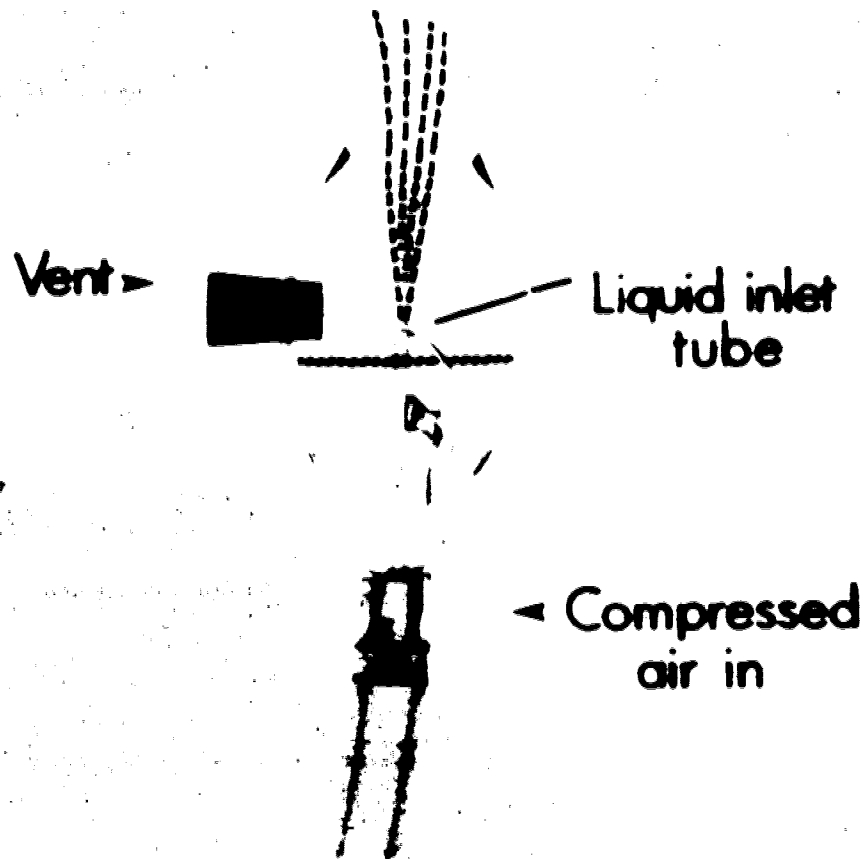


Fig. 1 Diagram of the DeVilbiss model 40 nebulizer

The air flow accelerates the droplets, imparting sufficient momentum to impact the larger droplets on the throat of the nebulizer. More than 99% of the total droplet mass is returned to the solution in this manner with only the remaining 1% able to follow the air flow out of the nebulizer. The kinetic energy that is provided by the

impaction of the droplets on the wall is retained as thermal energy. It is offset by the loss of energy in the evaporation of solvent which saturates the outgoing air. The nebulizer then cools until an equilibrium temperature is reached. The evaporation of solvent causes a continuous increase in the concentration of solute in the liquid remaining in the nebulizer. This in turn increases the concentration of airborne solute in the useful aerosol and shifts the size distribution of the residual solute particles to larger values.

The effect of opening the vent on the DeVilbiss model 40 is two-fold. First, it increases the gross output of useful aerosol per minute by up to a factor of 2. At the same time, however, it also increases the mass median diameter of the droplet distribution by 25 to 30% (30). Second, the added vent air does not carry away relatively as much as the jet air so that there is a decrease in the concentration of the useful aerosol. This shows that a portion of the droplets returned to the bulk solution are actually within the useful size range but are not carried away by the jet air stream.

The mass median diameter (MMD) of the droplet distribution of useful aerosol at the time of formation, along with jet flow rates and pressures to the nebulizer as provided by Mercer (48,30), are included in Fig. 2 and summarized in Table I. The MMD values in Table I were taken from Rabbe, but conform well to Mercers data in Fig. 2.

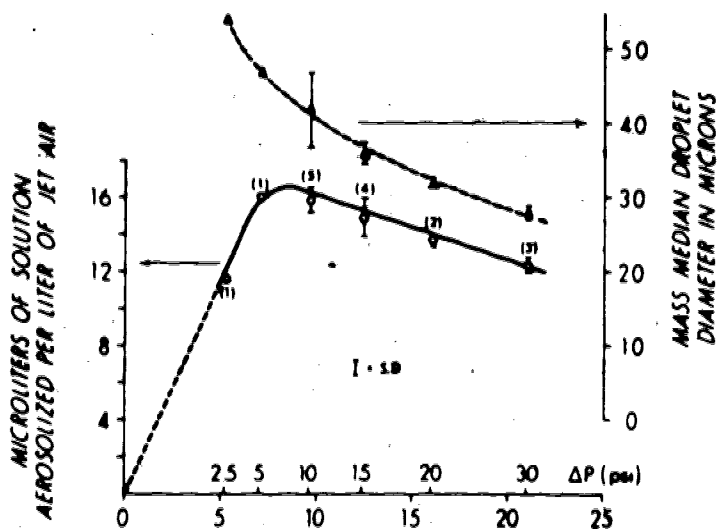


Fig. 2 - Output and mass median diameter as functions of jet flow rate for the DeVilbiss 40 nebulizer (48).

TABLE I

OPERATING AND OUTPUT CHARACTERISTICS OF THE DEVILBISS
NEBULIZER (VENT CLOSED) (30)

Pressure Drop (PSIG)	Flow Rate l/min	Equilibrium Temp C°	Output in μl/l Jet Air		Volume Median Droplet Diameter μM	MMD (μM) (41)
			Aerosol	Water Vapor		
15	12.4	10.4	15.5	8.6	4.2	3.5
20	16.0	10.0	14.0	7.0	3.2	3.2
30	20.9	9.3	12.1	7.2	2.8	2.8

*Geometric Standard Deviation 1.8-1.9

Ultra Sonic Nebulizers

Ultra sonic nebulizers convert the vibrations from a piezoelectric crystal to a coupling liquid, then to the solution to be nebulized. The ultrasonic energy is intense enough to create a fountain of liquid from which a fog of very small droplets is produced.

Sollner's (42) work on ultrasonic atomization led him to conclude that the mean size of the droplets in the fog is a function of the frequency of the crystal. The frequency of oscillation ω , of the crystal is related to the capillary wavelength λ , on the surface of a liquid of surface tension σ , and liquid density ρ as follows:

$$\lambda = (8\pi\sigma/\rho\omega^2)^{1/3} \quad \text{Eq. (5)}$$

where σ is in dynes/cm, ρ is in g/cm³ and ω is in Hz.

Lang (43) then demonstrated that the count median diameter (D_{og}) of the droplets produced is directly related to the capillary wavelength by

$$D_{og} = 0.34 \lambda \quad \text{Eq. (6)}$$

This relationship has been found to hold for frequencies between 12kHz and 3MHz (44), the range of most commercial ultra-sonic nebulizers.

The concentration of particles in the aerosol cloud *

generated by ultrasonic nebulizers is generally about 100 times that of air blast nebulizers, although the aerosol output in ml. of solution per minute is only slightly higher. The particle size produced by most commercial nebulizers is larger than those of the air blast system and is generally in the range of 5 to 10 μm (MMD).

There have been several papers written on performance data for both air blast and ultrasonic nebulizers which summarize the characteristics of some commercially available systems (45-50).

Dispersion of Dry Powders


While dry particles can be dispersed by simply blowing air through a loose mass of powder, there is difficulty in preventing clumping and maintaining a uniform particle size. The most successful systems for dispersing dry powders involve abrasion of a plug of compacted powder either by compressed air or by mechanical scrapers.

PARTICLE SIZING

Introduction

There are numerous methods available for the sizing of particles in the range of interest in a pulmonary study (i.e., 0.5 to 15 μm). In practice particle sizing can be done by two methods: 1) geometric measurements (volume or shape factors) and 2) aerodynamic measurements. Techniques used to measure particle size in the former include electron microscopy, photometric, nucleopore and millipore filtration, light microscopy, Coulter counting, and ultracentrifugation. The method preferred is the aerodynamic measurement which relates the particle size to its aerodynamic properties. This measurement generally takes into account several physical characteristics of the particle including shape, density, and resistance to flow. It equates the particle to an equivalent spherical particle of unit density by means of analytical or empirical relationships.

Methods based on inertial or terminal settling velocity give rise to the inertial or aerodynamic size (often referred to as Stokes' diameter, where the diameter is calculated by assuming Stokes' Law). Aerodynamic diameter is accordingly defined as the diameter of a sphere of unit density having the same terminal velocity as the particle in question, regardless of its shape, size, or density. The Stokes' diameter is defined as the diameter of a sphere having the same density and Stokes' drag as the particle in



question, or more specifically, the diameter of a sphere with the same terminal settling velocity and density as the particle in question.

Merely stating the average diameter of the particles in any aerosol experiment is not sufficient. As most aerosols contain a wide range of particle sizes, a knowledge of the size distribution and a mathematical expression to describe it are highly desirable, especially when it is necessary to estimate particulate characteristics that are not measured directly.

Many analytical relationships have been proposed representing the size distribution of an aerosol, notably the Rosen-Rammler, the Roller, the Nukiyama-Tanasawa, and the log-probability distribution. Of these, the lognormal or log-probability distribution is most widely used in aerosol studies and it is this relationship that we will discuss. Thus, the lognormal distribution is merely the normal distribution applied to logarithms of the quantities actually measured. An aerosol is said to be lognormally distributed if the particle distribution in which activity (radioactive or solute concentration) is normally distributed with respect to the logarithms of the particle diameters.

The most convenient method of representing the aerosol distribution is a graphic plot on log probability paper of cumulative percent against particle size (Fig. 3):

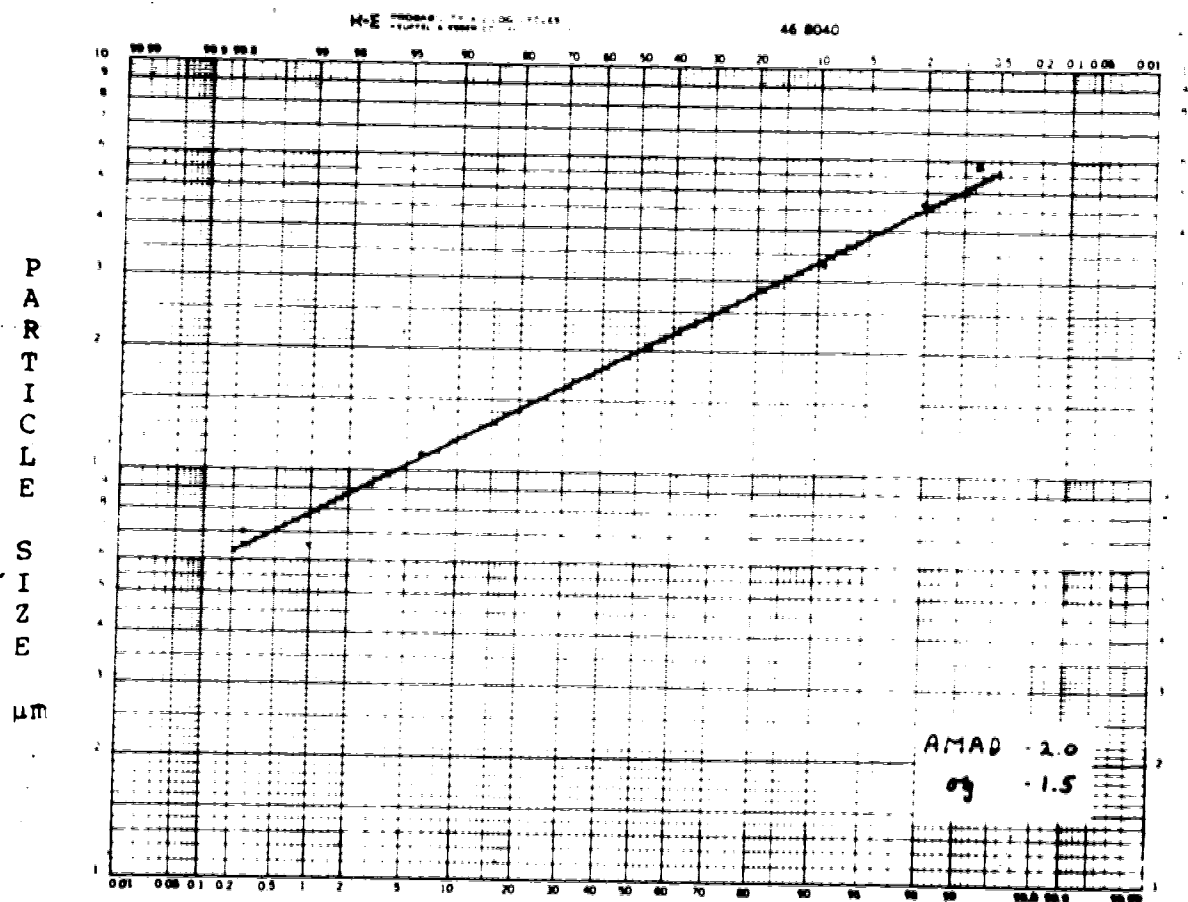


Fig. 3 A lognormal plot of a particle size distribution.

If the size distribution follows a log-probability relationship, the plot of cumulative percent against particle size will yield a straight line. Thus, the size distribution can be characterized by two numbers: 1) the median diameter, corresponding to the 50% cumulative size; and 2) the geometric standard deviation, a number equal to unity for a perfectly monodispersed aerosol and given by the ratio of either the 84.13% to the 50% or the 50% to the 15.87% cumulative size.

The median diameter, D_m , is a measure of the general size level, whereas the geometric standard deviation (σ_g) is a measure of the degree of uniformity. In terms of a specific property, X , half the material is finer than the median size (D_m), the other half coarser. In the case of the most common measurement, mass, a mass median diameter (MMD) will have one half of the mass above the specified diameter, the other half below.

In addition to the MMD, it is also sometimes desirable to plot number (also known as count), or surface-area data to determine these particle diameters. On single plot, each of the parameters would run parallel to each other and have the same geometric standard deviation as the number distribution and vary only with respect to the aerodynamic diameter value.

For illustrative purposes a schematic lognormal distribution curve is shown in Fig. 4 to demonstrate the relative positions of the various particle parameters. The same data are also illustrated on a log-probability plot in Fig. 5. Both graphs were taken from the Handbook of Aerosols (89).

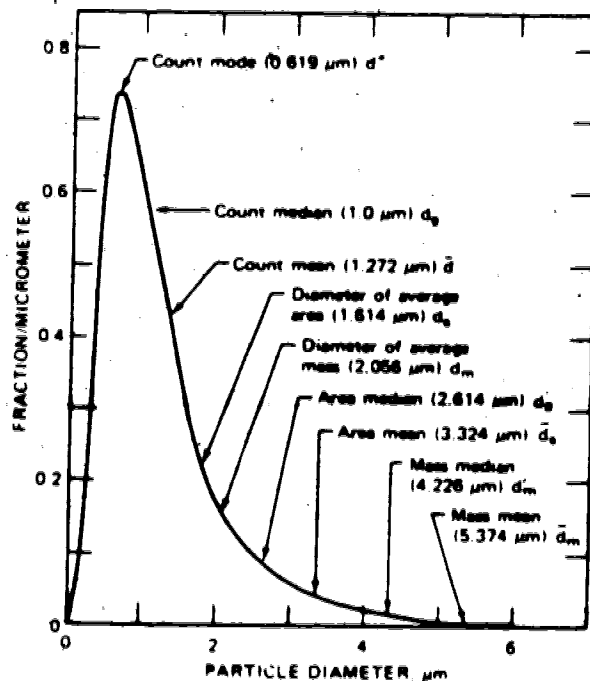


Fig. 4 - An example of the lognormal distribution function in generalised linear form for $d_g = 1.0$ and $\sigma_g = 2.0$.

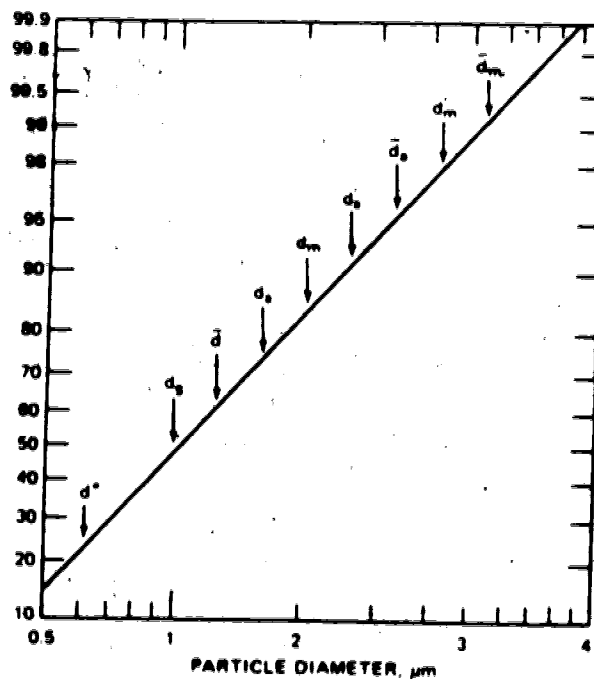


Fig. 5 - Size distribution plotted on lognormal probability paper for $d_g = 1.0$ and $\sigma_g 2.0$.

Cascade Impactors

Instruments employing the process of impaction have been used for many years to sample toxic airborne particles. Early models were plagued with problems of rebound, re-entrainment and disaggregation (51). May (52) introduced a system of segregating particles into several fractions, each of which contained only particles having sizes between more or less sharply defined limits. Since then, the impactor has become one of the most widely-used instruments for the study of particle size in relation to inhalation toxicity.

Cascade impactors allow direct determination of the cumulative distribution of particle activity as a function of aerodynamic size. The accuracy with which such distribution can be estimated from cascade impactor data depends on the degree to which the size distribution of particles passing a given impaction stage overlaps the size distribution of particles retained in that stage.

The Andersen cascade impactor (Andersen Samplers Inc.; Atlanta, Ga) classifies the particles collected according to their aerodynamic diameter within the range of 0.4 μm to 9.8 μm . The instrument has been designed and calibrated with unit density spherical particles so that all particles, regardless of their physical size, shape, or density, are sized aerodynamically equivalent to the reference particles.

The Andersen impactor consists of eight stages having smaller orifices and progressively less area on each stage

for the airflow to traverse. Accordingly, the airflow through each stage is increased and the particles will be given a greater momentum on passing through each stage. If they are given sufficient momentum, they will impact on a collection plate located between each set of stages. An absolute filter follows the last stage to collect all particles below 0.4 μm which have escaped impaction.

Such a system is intrinsically limited in defining any size distribution by the number of stages it incorporates as well as by the reliability of the analytical method. Thus, in practice, the system is not 100% efficient for trapping only those particles to which it has been calibrated. For all but the most exacting work, however, the Andersen impactor has proven to be quite satisfactory.

When analysis of the sample plates is carried out by gravimetric methods, the sizing of the test aerosol gives rise to a measure of the mass median aerodynamic diameter (MMAD). For a sphere, the MMAD is related to the MMD by the relationship (53):

$$\text{MMAD} = (\text{particle density})^{1/2} \text{MMD}. \quad \text{Eq. (7)}$$

When radioactive particles are used, analysis can be carried out by gamma or beta counting to determine the activity median aerodynamic diameter (AMAD). Providing that there is an even distribution of the radioactive agent throughout the volume of the droplets, the AMAD will equal the MMAD.

The Effect of Ionic Concentration on the Size of Aqueous Aerosols

The initial composition of the liquid to be nebulized is extremely important in the determination of the size of particle which will enter the lungs. In the case of pure deionized water the lifetime of the smaller droplets is extremely short, even at high humidities as Table II shows.

TABLE II (54)

CALCULATION OF EVAPORATION TIMES OF ISOLATED WATER DROPLETS IN AIR OF DIFFERENT HUMIDITIES AT 21 °C AND 760 mm PRESSURE

Diameter of water Droplet µm	Time for Complete Evaporation at Relative Humidities of				
	100%	99%	90%	50%	0%
	Seconds	Seconds	Seconds	Seconds	Seconds
50	16,200	69	6.9	1.38	0.69
20	1,040	11.1	1.11	0.22	0.111
10	129	2.8	0.28	0.56	0.028
5	16.2	0.69	0.069	0.0138	0.0069
2	1.04	0.111	0.0111	0.0022	0.00111
1	0.129	0.028	0.0028	0.00056	0.00028

Based on theoretical models, an equation can be derived which relates droplet diameter (d) at time (t) to its original diameter (do) at time 0.

$$d^3 = do^3 - 13.13 \mu\text{m}^3/\text{sec} \cdot t \text{ sec} \quad \text{Eq. (8)}$$

@ 298 K + 100% R.H.

The equation is valid for particles $\geq 0.1 \mu\text{m}$ (55).

It must be pointed out that this equation is only valid for isolated water droplets. In an aerosol cloud, however, Reif (54) points out that the vapour pressure of the atmosphere will rise rapidly as the smaller droplets evaporate. This will be counterbalanced by a corresponding decrease in the evaporation rate of the remaining larger droplets as equilibrium saturation is approached within the cloud. Table III shows that the degree of supersaturation is only slightly above 100% R.H. for droplets larger than $10 \mu\text{m}$ in diameter.

TABLE III (54)

PER CENT SUPERSATURATION OF THE ATMOSPHERE REQUIRED TO HOLD, IN EQUILIBRIUM, ISOLATED WATER DROPLETS OF VARIOUS SIZES

Diameter of Water Droplet μm	Percentage Supersaturation	
	at 0 °C	at 21 °C
50	0.005	0.004
20	0.012	0.011
10	0.024	0.021
5	0.048	0.043
2	0.120	0.107
1	0.240	0.214

Since there are time intervals between 0.5 and 2 seconds between production and inhalation (depending on the type of equipment used) of an aerosol from a nebulizer, one can visualize how important it is to understand the behavior of the aerosol cloud during this period. Porstendorfer (55) demonstrated that the pure water droplet size distribution, from a Bird compressed air nebulizer changed considerably in the first 1/10 second both in terms of concentration and net particle diameter.

The behavior of an aerosol is altered considerably by the introduction of substances into aqueous solution. Porstendorfer (55) discussed the size distribution changes which occur in solutions containing between 0.0002% NaCl up to 0.5% NaCl. Interestingly, the higher concentrations (above, say, 0.1%) have little effect on the droplet size at $t=0$ from the size distribution obtained from a pure water aerosol at $t=0$. The very low concentration of 0.0002% (which is representative of the ion concentration in tap water) decreases the mean droplet diameter by about a factor of 10.

Perhaps more important is that, in contrast to pure water droplets, the solution droplets are relatively stable with respect to time. This is due to the vapour pressure elevation (Kelvin effect) on the droplet's surface brought about by the presence of the dissolved salt (55). Estimates show that 90% of the diameter change occurs within 10^{-1} to 10^{-3} seconds, values similar to those found for the pure

water droplets. The significance of this is that any sizing done on the aerosol solution by conventional impactor methods will be representative of the particle distribution for a significant period of time after formation of the aerosol.

One further factor which must be considered is the effect of taking an aerosol solution to its dry state. While it may be desirable to reduce the particle size by this method, Dautrebande and Walkenhorst (56) estimate that the particle may reabsorb water as it enters the lung, increasing in size by up to a factor of 7. In general, an increase of dry particle size must be expected for all aerosol particles which are soluble in water.

The rate at which this growth occurs is due primarily to the particles' initial size. Particles with an aerodynamic diameter smaller than $0.2 \mu\text{m}$ reach equilibrium size in the lung within 0.1 seconds, $1.0 \mu\text{m}$ particles require about 2 seconds, and $2 \mu\text{m}$ particles take 10 seconds. These figures apply to the most common salts; however, deviations can be expected for organic compounds (57).

PARTICLE DEPOSITION

Mechanisms of Deposition

Particle deposition in the lung occurs by one of these mechanisms:

- 1) inertial impaction
- 2) gravitational sedimentation
- 3) Brownian diffusion

The size of the particle most likely determines the mechanism by which a particle deposits in the normal lung. Large particles are most likely to deposit by inertial impaction. Landahl et al (58) state that there is a 33% probability of deposition by impaction for 7 μm particles, 10% for 3 μm , and 1% for 1 μm . The probability of inertial deposition, I , is proportional to

$$I \propto \frac{V_t V \sin \sigma}{gR} \quad \text{Eq. (9)}$$

where V is the velocity of the air stream, V_t is the terminal settling velocity of the entrained particle, σ is the angle of bend, R is the radius of the airway and g is the gravitational constant. Accordingly, by increasing particle size, air velocity, or bend angle or by reducing the airway radius, you would increase the probability of deposition by impaction. For example, if a 1 μm unit-density particle travels with an airstream moving at 0.2 m/sec (typical of center-stream air velocity in bronchi), then a 30° change in the direction of air flow will move the

particle 0.3 μm away from its previous streamline (59).

Particles with a density greater than that of air will experience gravitation settling or sedimentation (the second important mechanism in lung deposition). A particle will accelerate downwards until it reaches its terminal velocity, V_t , a value at which the resistance to its downward motion through the air is balanced by its weight. V_t is related to σ , the particle density, d , its diameter, γ , the viscosity of air, ρ , the density of air, and g , the gravitational constant by the relationship

$$V_t = \frac{(\sigma - \rho) g d^3}{18\gamma} \quad \text{Eq. (10)}$$

Again considering a unit-density, 1 μm particle, falling through air at atmospheric pressure and body temperature, a terminal velocity of 33 $\mu\text{m}/\text{sec}$ would be reached in 10 μs if $V_0 = 0$. For particles less than 1 μm the mean free path of air begins to approach the particle size and must be accounted for by the Cunningham slip correction factor.

Landahl (58) uses the terminal settling velocity S , to calculate the probability of deposition in the lung by relating it to t , the time travelled along a given airway of angle ϕ to the horizontal, and a radius R of the airway by:

$$S = 1 - e^{(-0.8v_t \cdot t \cdot \cos \phi)/R} \quad \text{Eq. (11)}$$

Sedimentation is likely to be the most dominant factor of deposition at the smaller bronchi and bronchioles, affecting particle sizes down to an MMD of about $0.5 \mu\text{m}$.

On the other hand, diffusion or Brownian motion will affect particles ranging from $0.5 \mu\text{m}$ to less than $0.005 \mu\text{m}$ and occurs principally in the parenchyma. Brownian (thermal) motion of very small particles is due to the random "jostling" due to collisions between gas molecules and the aerosol droplets. The magnitude of this displacement, Λ is a function of time, t , C , the Cunningham slip correction factor, γ the gas viscosity, d particle density, and the gas constants NRT . The relationship is given by:

$$\Lambda = \left(\frac{RT}{N} \cdot \frac{Ct}{3\pi\gamma d} \right)^{1/2} \quad \text{Eq. (12)}$$

A unit-density $1 \mu\text{m}$ sphere would move $13 \mu\text{m}$ in 1 second as a result of diffusion.

The probability of particle deposition D by diffusion increases as the displacement increases relative to the dimension R of the confining space; hence, D is proportional to Λ/R , and Landahl (60) developed the relationship

$$D = 1 - e^{-0.58 \Lambda/R} \quad \text{Eq. (13)}$$

to describe this probability. Thus, as Λ increases, the probability of deposition approaches 100%, while Λ increases

with time and decreases with size. The effectiveness of deposition by diffusion increases with decreasing particle size, but with decreasing particle size, the probability of deposition by gravitational settling decreases, and so a size of minimum deposition results and corresponds to an MMD of about 0.5 μm . These processes are discussed in detail by Hatch and Gross (61).

It is often assumed that particle deposition will parallel pulmonary ventilation; however, this may not be the case, especially in patients with lung disease. Deposition refers to the initial processes that determine the fraction of the particles in the inspired air which are caught in the lungs and fail to exit with the expired air. The properties responsible for deposition of a particle onto an airway surface are only partly related to the air volume within that airway. For small particles, factors such as turbulence, bifurcation angles, and residence time in an airway (all of which may vary regionally within the lungs) will affect deposition, yet be independent of the ventilation of the region.

Regional Deposition

One of the first requirements in dealing with a lung model is a definition of the regions of the respiratory tract. The Task Group on Lung Dynamics recommended the following description (16).

- 1) The nasopharynx (N-P) -- this begins with the anterior nares and extends through the anterior pharynx, back and down through the posterior pharynx (oral) to the level of the larynx or epiglottis. This compartment corresponds to the established medical description of the upper respiratory tract. However, we regard this term unimportant for the lung model.
- 2) Continuing caudally, the next compartment, (T-B), consists of the trachea and the bronchial tree down to and including the terminal bronchioles. Compartments 1 and 2 together constitute the anatomical dead space of the respiratory tract. Also, together they can be considered as representing the entire epithelial area of the respiratory tract which is ciliated and covered with mucus arising from two elements, goblet cells and secretory cells.
- 3) The third compartment is pulmonary (P). This region consists of several structures, viz. respiratory bronchioles, alveolar ducts, atria, alveoli and alveolar sacs. The exact names and descriptions vary somewhat according to different authors and sources (62,63) but in all cases the region can be regarded as the functional area (exchange space) of the lungs. Its surface consists of non-ciliated, moist epithelium with none of the secretory elements found in the tracheobronchial tree. Compartments (T-B) and (P) together constitute what has been termed the lower respiratory tract, but this term serves no useful purpose in the proposed models.

The total deposition (D_T) of an inhaled aerosol is the sum of regional depositions; i.e.,

$$D_T = D_{NP} + D_{TB} + D_P$$

Eq. (14)

where D_{NP} , D_{TB} and D_p are the regional depositions in each of the 3 areas previously discussed.

The Group has provided a description of the regional deposition at a given mass median aerodynamic diameter in each compartment (Fig. 6). The range or envelope given for each region is the variation which can be expected when the σ_g varies from 1.2 to 4.5. The data are for a tidal volume of 1450 ml. (No inhalation rate information was given).

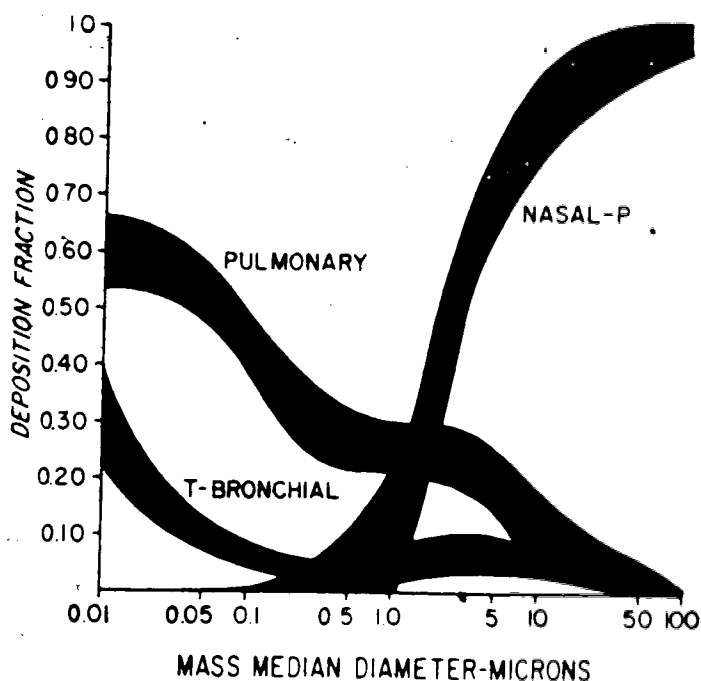


Fig. 6 - Deposition fraction in each of the nasopharynx, tracheo-bronchial, and pulmonary regions of the lung for a given MMAD when σ_g varies from 1.2 to 4.5 and tidal volume is 1450 ml.

Reprinted with permission from Pergamon Press Inc. and the Health Physics Society (16).

There is much better agreement in the literature on the division of regional deposition for a given particle size than there is for total deposition. The first studies were carried out by Hatch and Hameon (1948)(64), Welan and LaMer (1948)(65), Gessner (1949)(66), Brown (1950)(67) and Beeckmans (1965)(68) who developed a theoretical model in which airways were represented by a system of branching tubes.

More recently Stahlhofen et al (69) who claim to have improved on Lippmann and Albert's technique conclude that up to an aerodynamic diameter of about $2.4 \mu\text{m}$, particle deposition only occurs in the alveolated (Pulmonary) region under normal breathing conditions. They add that this deposition is due to gravitational settling. Yu and Taulbee (70) confirm their findings and point out that there is only a slight increase in the tracheobronchial deposition when the tidal volume increases from 250 cm^3 to 500 cm^3 and T-B deposition remains nearly constant for tidal volume above 500 cm^3 . They further stated that any increase in total deposition is due mainly to the increase of deposition in the pulmonary compartment.

For particles in the range of 0.5 to $3.0 \mu\text{m}$, Yu and Taulbee provide a theoretical profile of the deposition fraction vs. airway generation (Fig. 7). This study was done for a tidal volume of 500 cm^3 and a breathing rate of 15 breaths/min.

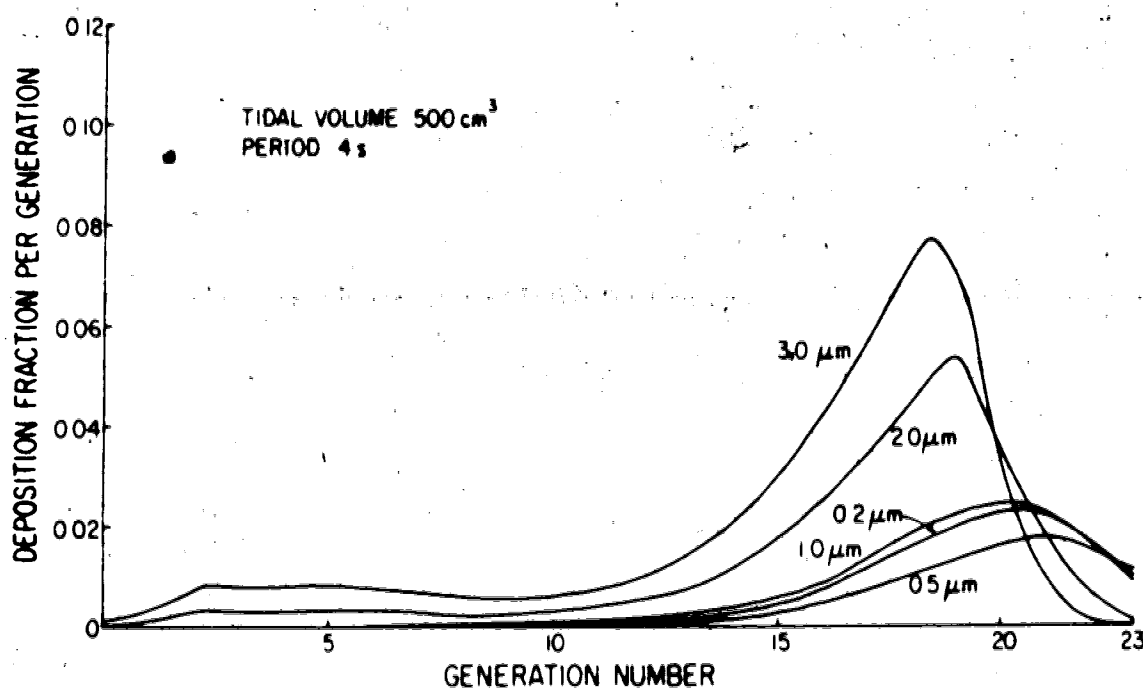


Fig. 7 - Theoretical prediction of deposition profile along the respiratory tract at 500 cm³ tidal volume and 4-second breathing period for various particle diameters.

Reprinted with permission from Pergamon Press and the Institute of Occupational Medicine (70).

Total Deposition of Particles in the Lung

The total deposition of inhaled particles appears to be the most variable of the parameters relating to aerosol deposition in the lung. This is due, in part, to the large number of factors which can affect particle deposition. These include the aerodynamic size of the particles, the shape of the particles, especially when the shape deviates

considerably from spherical (such as asbestos fibres), the hygroscopicity, the inhalation flow rate, tidal volumes, electrostatic forces, and the presence, extent, type, and degree of disease in the lungs.

The experimental results on total deposition were recently reviewed and discussed by Davies (71). He has shown there is an unacceptable amount of scatter, due not only to the usual difficulties with aerosol experiments but also to the uncontrolled breathing and physiological conditions of the subjects.

Recent studies have attempted to control these conditions more carefully. (Muir and Davies, 1967; Davies et al., 1972; Heyden et al, 1973, 1975, unpublished, as cited by Yu and Taulbee (70)).

In a joint study between the aerosol groups of GSF at Frankfurt and CNEN at Bologna (72), closely controlled trials reduced errors to the limit of intersubject variability. Their aerosol consisted of monodispersed di-2 ethylhexyl sebacate droplets generated by condensation of vapours on ferric nuclei by the hot wire technique. Particles of 0.6, 1.0, and 1.5 μm (and a density of 0.91 gm/cm^3) were investigated and measurements of total deposition were taken.

In this study sizing was carried out by at least two of following methods: electrical mobility spectrometer, a sedimentation cell, or a light scattering spectrometer. The modal diameter of the monodispersed aerosols using the

different analytical techniques always agreed within 5%.

Total deposition was measured by the Bologna group through monitoring of the particle number concentration in the inspired and exhaled gas by photometers. The Frankfurt group utilized a pneumotachograph and a light scattering photometer to measure flow rates and particle concentration.

Also investigated were the effects of charge (as generated by a corona discharge system and measured by the electrical mobility spectrometer) on deposition of $0.6 \mu\text{m}$ particles. The results of this study are summarized below.

- 1) Deposition was found to be independent of particle material (carnauba wax and di-2-ethylhexyl sebacate particles).
- 2) Although subjects initiated inspiration of aerosols from their individual functional residual capacities, intersubject variation of deposition was observed. At $1.5 \mu\text{m}$ the range of total deposition on 4 subjects ranged from about 13% to 25% at inspiratory rates of 15 l/min and V_t of 500 cm^3 . At inspiratory rates of 30 l/min and V_t 1,000 cm^3 , the deposition of $1.6 \mu\text{m}$ particles ranged from 17% to 30% and at rates of 15 l/min. and V_t of 2,000 cm^3 , deposition varied from 58% to 65%.
- 3) Deposition was not affected by 2 or 3 elementary charges carried by the wax particles.
- 4) Additional charging of the particles, however, led

to an enhanced deposition and this increased with increasing charge.

This report agrees quite well with the study of Davies and co-workers (1977)(73) who have developed a formula that expresses total deposition of particles in the size range from 0.5 to 2.5 μm , as a function of tidal volume, breathing frequency, particle size, and one parameter which is subject specific. Within this size range, deposition increases from 10 to 60% with increasing tidal volume and decreasing breathing frequency.

Particle Clearance

It has been pointed out in the previous discussion, both in theoretical models and in experimental studies, that in normals particles below a size of about 3 μm demonstrate minimal deposition in the T-B region. Accordingly, particle clearance via the mucociliary system from this region for the smaller particles is correspondingly low.

Regional deposition patterns shift, however, in subjects with obstructive pulmonary disease (74,75) and, to a lesser extent, in smokers (20,76). The shift of deposition from the pulmonary compartment to the T-B region can result in a much higher central deposition fraction and a marked increase in clearance from this area.

Several investigators have used gamma cameras or scintillation detectors to measure the extent and rate of T-B clearance (20,74-78). From these measurements, estimates

of the relative deposition in the two regions were obtained as it is assumed that mucociliary clearance is effectively completed by 24 hours.

Lippmann and Albert (79) investigated deposition of particles in the size range 2.1 to 12.5 μm (σ_g 1.08) in normals. They used the proportion of the initial lung burden of radioactive particles removed during the first 24 hours to provide a functional measure of tracheobronchial deposition. They had insufficient data for particle size below 4 μm to determine the size dependence on fractional deposition in this region. One of their main conclusions was that there were large differences between individual subjects in the amount of deposition at any given particle size. It should be noted that the only controlled breathing parameter in their study was that of breathing frequency.

Albert et al (15) conducted a study which compared clearance in smokers and non-smokers. Again the bronchial tree deposition was highly variable with the smaller particles even when breathing frequency was regulated (14 breaths/min) and inspiratory flow rate varied only marginally. One study showed that for 2.5 μm particles inhaled by 5 subjects, the % retention over 24 hours varied from about 20% to 75%. In comparing smokers and non-smokers they noted that "By far, the most striking abnormality in the behaviour of inhaled aerosols is the remarkable increase in the aerosol deposition efficiency of the bronchi in some smokers and most bronchitics (15)."

The wide variation observed between particle deposition in the T-B and P regions for particle sizes between roughly 2-7 μm , even in experiments which carefully monitor the breathing parameters, confirms this large inter-subject variability. A study by Matsuba and Thurlbeck (80) on the size of small airways in 20 normal cadavers found a coefficient of variation of 0.24. Given this large value, a considerable range of clearance rates can be expected between normal individuals for reasons based solely on their anatomical variability. In order to maintain the inter-subject variability at a minimum, breathing patterns and aerosol parameters must be controlled and monitored carefully.

Regional Variations in Aerosol Deposition

Most researchers have dealt with "regional deposition" within the lung by referring to the distribution of particles between the tracheal-bronchiole region and the pulmonary region as defined by the Task Group on Lung Dynamics. The general attitude is that there is a homogenous distribution of particles in these two regions throughout the lung. Both theoretical and animal trials have shown that this is not the case.

Theoretical Models

Using a silastic cast molded from a human lung, Schlesinger and Lippmann (23) investigated the deposition

patterns of 3.5 to 12.2 μm particles in the lung. Although their model only extended to the segmental bronchi, they found that most deposition occurred at airway bifurcations. It was also noted that while total deposition varied with particle size (approximately 50% for 11 μm particles vs. 4% for 3.5 μm particles), the areas of impaction remained relatively the same.

In a later paper Schlesinger and Lippmann (81) reported a close correspondence between relative deposition efficiency and frequency of reported cancer at those sites. They suggest that the deposition characteristics of the airways may play a significant role in cancer pathogenesis. Their model was again a silicone rubber cast of the tracheobronchial tree but in this experiment it extended down to 2 mm airways. Their particles varied from 1.7 to 12.2 μm . This model confirmed their first study which noted that areas of impact were similar for all sizes of particles and for different flow rates.

In another recent study, Shaw et al (24) found the peak deposition flux is higher than the average deposition flux by a factor ranging between 5 and 30, depending on particle size and generation number. They also observed that smaller particles had higher peak-to-average deposition fluxes than did larger ones because the particle deposition of small (<2 μm) particles is caused primarily by sedimentation which does not create hot spots near the bifurcations. Based on Yu and Taulbes' calculations that a 2 μm particle is most

likely to deposit around the 18th generation, Shaw indicates a peak-to-average deposition ratio in this region of about 7 to 1 for this size of particle.

Animal Studies

One of the first long-term retention measurements was carried out by Stokinger (11). Using two particle sizes of uranium dust (2.6 and 0.45 μm) he found total deposition was 10 times larger for the smaller particles. Another significant observation was that the superior segment of the right lobe had 150 to 175% greater deposition than any other region. These differences were observed in all rats, irrespective of the dust type (U_3O_8 or UO_2) or particle size. Their clearance measurements also showed two interesting findings. First, the right middle lobe had essentially no clearance for the first 10 days post exposure and second, there was a faster clearance from the superior right lobe. The biological half life for the larger and smaller particles was 3 months and 8 months respectively.

Thomas and Raabe (12) conducted a study to determine the regional deposition of mono- and polydispersed aerosols in two groups of Syrian hamsters. Their experiment showed that the lung deposition expressed as a fraction of inhaled aerosol was the same for similar sizes of mono- and polydispersed aerosols. In addition, in every case, the right apical lobe had the highest concentration of deposited particles and the right cardiac and diaphragmatic lobes, the

lowest.

This finding was confirmed by Brain's (13) group who did testing on both rats and hamsters. They divided the left lung into six, approximately equal, sections on both species. The right lung was sectioned into 17 sections according to its lobar regions. They observed that the regions of greatest activity per unit weight occurred in the apical regions and decreased towards the basal regions. Brain et al also noted that there were little deposition differences between the two groups of rodents (13).

The three animal studies reported base their calculations on an activity per unit weight of lung tissue. None of the authors corrected for blood concentration in their samples.

GAMMA CAMERA EMISSION TOMOGRAPHY

There has been considerable progress made in medical imaging over the past few decades. One of the significant developments in the field of nuclear medicine has been single photon emission computed tomography (SPECT). This technique has only recently become popular with the introduction of commercially available rotating gamma camera systems. SPECT should, in principle, provide better visualisation, and possibly quantification, of the 3-dimensional distribution of radiotracers within patients. In most cases, this can be done without an increase in the administered dose.

The first rotating gamma camera system available in North America was the General Electric 400T (G.E., Milwaukee, Wisconsin). The camera is capable of moving around the patient taking a series of 32, 64, or 128 images at equal intervals in a 360 degree rotation. Tomographic images are usually reconstructed using a technique referred to as filtered backprojection (82).

The numerical data for the reconstruction programme comes from a series of "digital" images acquired during the rotating scan. The digital image, or matrix, is composed of a square array of "pixel's" (picture elements). Each pixel contains a numerical value representing the photons observed from a specific region of the gamma camera face. The area represented by each pixel is a function of the matrix size, and field of view of the camera. For example, given a 64 x

64 matrix imaged on a camera head of 40 cm diameter, the theoretical width of a pixel would be 0.626 cm.

The quality of the reconstructed image obtained will depend on several factors. These include the size of the acquisition matrix, the number of angles used during the acquisition and the total number of counts acquired in all of the images. More practical factors which also affect image quality are the amount of subject movement during acquisition, the energy of the radionuclide used, the type and degree of filtering incorporated into the reconstruction, and the thickness and gamma ray absorptive characteristics of the object being imaged.

The ultimate resolution obtained in the tomographic reconstruction will depend on the above and additional factors, such as the distance between the camera face and the object being imaged, the type of collimator used, and even the length of coaxial cable connecting the camera to the computer. Depending on how these parameters vary, the resolution (FWHM) can vary from 9 to greater than 20 mm (83) even using the most sophisticated reconstruction programmes (82).

For a variety of reasons, noise is higher in tomographic reconstruction than in conventional scintigraphic views at comparable count densities. This noise can be reduced to some extent by filtering but such filtering also decreases resolution.

One important consideration is that tomographic

reconstructions do not necessarily reflect the true count densities inside the object being scanned. Tomographic sections are more sensitive to uniformity artifacts than are conventional views. In one of Larsson's experiments (82), he found that a 10% (cold) artifact produced a 12% variation in a static anterior view but a 28% difference in the tomographic section. The corresponding values obtained with a 22% artifact were 33 and 52% respectively. He also states that the extent of the variation of the artifact measurements were strongly dependent on the gamma camera uniformity. The G.E. 400T, however, has a built-in uniformity correction which should minimize this source of error in the reconstruction.

CHAPTER III

EXPERIMENTAL

PARTICLE GENERATION AND SIZING

Several trials were conducted, varying the operating parameters and system design characteristics of a variety of nebulizers. The two basic systems for producing polydispersed aerosols, namely air-blast and ultrasonic nebulizers, were investigated and particle size measurements were made on the aerosols produced. In addition, several different compounds labelled with ^{99m}Tc were screened for possible application in either the human or animal trials.

A summary of the tests carried out on the Bendix Ultrasonic Nebulizer is listed in Table XI of the appendix. The Bendix Ultrasonic Nebulizer operates on a fixed frequency of 1.26 MHz. Theoretical calculations based on equations (5) and (6) indicate a count median diameter of 3.4 μm . Using the Hatch-Choate equation (2) and knowing the σ of the particle distribution (say, 1.4) we can calculate the theoretical MMD from the equation

$$\ln (\text{MMD}) = \ln (\text{CMD}) + 3(\ln \sigma)^2 \quad \text{Eq. (15)}$$

which corresponds to a value of 4.8 μm .

The container from which the bulk solution was nebulized was modified to allow smaller volumes of high specific activity radiopharmaceuticals to be used. Containers made from 20 cc. syringe cases proved adequate in conducting the ultrasonic waves and in nebulizing as little as 1 ml. of solution.

Particle diameters of the generated aerosol were larger, and geometric standard deviations smaller than those produced in the air-blast nebulizers. This larger particle size would have shifted the particle deposition towards T-B region, which in turn would have increased clearance. This would have served no useful purpose in these initial experiments therefore, the ultrasonic system is not used in the human trials. In addition, technical modifications would have had to be incorporated in order to allow measurements of the inspiratory flow rates and tidal volumes.

Three brands of air-blast atomizers were tested, again varying the operating parameters and technical layouts of the system. The brands tested were the Hudson, Model 1712 (Hudson, Temecula, Calif.), Airlife Mistyneb (Airlife, Inc.; Upland, Calif.) and the DeVilbiss models 40 and 45. Test summaries of the Hudson and Airlife designs are appended in Table XII. Again, these two models showed no particular advantages over the DeVilbiss model 40 which was ultimately chosen for nebulizing the aerosol in the human trial.

The DeVilbiss model 40 was one of the more common nebulizers on the market for many years, although it is now being replaced by their model 45. Tests and trials with this model were extensive and are presented in Table XIII (appendix).

Most tests were conducted using the bag-in-the-box to remove the larger droplets and to allow a uniform

distribution of radioactivity to reach the lungs. The Rudolf valve was replaced by the cascade impactor on most trials but on runs #12 and 14 the impactor was connected to the mouthpiece arm of the Rudolf valve in order to duplicate as closely as possible the experimental system as it would be arranged in the human trials (See Fig. 9 for an illustration of the aerosol generation system).

Aluminum is known to increase the particle size of sulphur colloid when it is present as a contaminant (84). Run #18 was an attempt to determine if larger particles of sulphur colloid could be produced by adding aluminum ions as a contaminant. Microscopic sizing of the initial solution indicated many particles in the 2 to 5 μm range; however, a sample of the nebulizer solution taken after the run showed very few particles larger than 1 μm , an observation in line with the impactor sizing of 1.6 μm . As the indications were that the particles produced by this method were unstable during nebulization, it was felt this technique could not be used for increasing particle size.

A similar situation was found when, mainly out of curiosity, a solution of macroaggregated albumin (MAA) was nebulized (run #19). The particles of MAA which are generally around 50 μm in diameter (85), were sized by impactor using gravimetric analysis and found to be 1.2 μm . Again a sample of the nebulizer solution indicated nearly all aggregates had been broken up into particles less than 1 μm with a few clumps in the range of 2 to 4 μm . This

is not entirely an unexpected result, however, considering the mechanism by which the aggregate is lumped together. The conclusion was again that the aggregates were unable to withstand the nebulization process.

Runs #7,8, and 9 illustrate that there is little if any effect on the particle size if the aerosol is retained in the bag for up to 45 seconds before being inhaled (or drawn into the impactor). The effective output of useful aerosol was reduced, however, by allowing the longer settling time as many of the particles would deposit by sedimentation in the bag during this time.

The pressure to the nebulizer was 30 PSI on most of the trials, and all experimental runs on the human subjects. The flow rate at this pressure was measured at between 23 and 24 l/min (with the inlet air at between 20 to 25% R.H.) by both spirometric and flow rates techniques. This corresponds to a value reported by Mercer (48) to be 20.9 l/min for the DeVilbiss at 30 PSI when operating on dry air.

A minimum value of about 1 ml. remains in the nebulizer after nebulization. This is due to the fact that this amount is in the upper portion of the nebulizer (in the spray or on the walls) at any given time during generation and, is accordingly, unavailable to the inlet tube for aerosolization. This 1 ml. is in effect the "dead volume" of the system and one of the primary reasons such a large initial activity must be used in the nebulizer.

A modification was made to the sulphur colloid solution towards the end of the human trials. One of the chronic difficulties experienced with the generation of sulphur colloid particles was the low efficiency of the nebulization of radioactive particles to the lung. Some particles were unavoidably lost to the bag-in-the-box, tubing, and the Rudolf valve, but even more significant is the loss of particles in the nebulizer itself. Often up to 80% of the initial activity would be found on the throat of the nebulizer where the mainstream of particles impacted on the wall. As these particles did not wash off with the stream of liquid returning back to the bulk solution, they would be effectively lost from the solution. What was even more distressing was that the amount of activity which would stick to the wall on any given run was highly variable and unpredictable.

It was recently discovered that the addition of 0.05 ml of 25% human serum albumin (HSA) to 2 ml of sulphur colloid would considerably decrease this "sticky" tendency and increase the efficiency of transfer of colloid to the subjects. The albumin also appears to mop up any free TcO_4^- remaining in the colloid solution. (There is generally 2 to 4% free pertechnetate remaining after the labelling of the sulphur colloid preparations).

Through the addition of this small amount of HSA, we are now able to reduce our initial activity in the nebulizer by a factor of 50 to 70% and still end up with the same

activity in the lungs. Since the addition of the albumin, activity output has remained consistent between runs, ranging from 30 to 35% of the original solution specific activity. A small change in the particle diameter, an AMAD of 1.30 and σ_g of 1.68 accompanies this technical change in the solution preparation. This change should not effect the deposition pattern or behavior of the aerosol to any observable degree.

It should be pointed out that particles, once deposited in the non-ciliated regions of the lung, do not change their location within the time frame in which scanning was carried out. In nearly all cases, measurable lung clearance via the mucocillary system was completed within two hours. For the 8 subjects who received scans at 6 hours, the amount of clearance averaged less than 5%. Successive scans on several subjects revealed no distinguishable change in the activity distribution when compared to the initial tomographic scan, indicating no change in the particle distribution over short time periods (6^ohours).

CALIBRATION OF THE CASCADE IMPACTOR

As there appeared to be some discrepancy between the observed particle diameter (AMAD of $1.2 \mu\text{m}$) and the literature value of $2.8 \mu\text{m}$ (MMD, see Table I) for the DeVilbiss nebulizer, two checks were run on the Andersen cascade impactor to attempt to rule out any error in the impactor or in the measuring technique.

The impactor is designed to operate at a flow rate of 1 cubic foot per minute (CFM) or 28.32 l/min. To insure that this flow rate was properly set, a calibration graph was constructed on a flow meter (Cole-Parmer, Chicago, Ill.). Using a ~~100~~ 1 Tissot spirometer as the calibration standard, air flows at various rates were monitored around the region corresponding to a flow rate of 28 l/min on the scale of the flow meter. The calibration graph obtained corresponded nearly exactly to the graph supplied with the instrument. The flow meter settings based on spirometry measurements indicated a setting of 72.6% vs 72.5% on the calibration graph obtained from the data sheet.

As a further check on the calibration of the impactor, monodispersed latex spheres (Coulter Electronics, Miami, Fla.) of a known diameter (MMD = 1.875) were nebulized by the DeVilbiss 40 nebulizer. As appended in Table XIII, run #28, the particles, sized by gravimetric analysis, had a MMD of $2.03 \mu\text{m}$ and a geometric standard deviation of 2.25.

The geometric standard deviation, which should theoretically be 1.0, is high for, possibly two reasons.

First, although one could see large quantities of particles on stages 4 and 5 (corresponding to end cutoff diameters of 2.1 and 1.1 respectively) and nothing on any other stage, it is suspected that there were a large number of impurities in the submicron size range. This is a possibility confirmed by Mercer (30) who, in referring to the production of latex particles, states that "residual particles create a nuisance background that is especially troublesome when light scattering methods of analysis are being used". Second, it is possible that multiples formed by coagulation during nebulization^u cause deposition on the upper stages of the impactor. The combination of these two factors would undoubtedly have played a role in shifting the size distribution of the true particles and accordingly produce a larger geometric standard deviation than expected.

PHANTOM MEASUREMENTS

Introduction

In addition to furnishing measurements of resolution of the imaging system, the phantom trials provided data critical in the analysis of two parameters of the human study. The first of these was to provide numerical values which could be used to deduce the variance or experimental error inherent in the measurements taken from the tomographic reconstruction. The second was to determine the extent and effects of attenuation, both from the internal absorbance factor as well as attenuation due to the patient couch.

A glass phantom was constructed from cylindrical glass tubing having an outside diameter of 178 mm and wall thickness of 4 mm. The length of the phantom was 275 mm (OD) and the volume, when filled, was slightly over 6 l (6.075 l). Six hollow spheres were placed inside to simulate lesions (Fig. 8). They were connected to the outside of the cylinder by 4 mm hollow tubing to allow access for filling. The spheres, arranged in 3 groups of 2, were placed at distances of 70, 120, and 170 mm from one end leaving about 100 mm free at the other. Each pair of spheres was spaced 30 mm \pm 1 mm center to center from each other with the upper sphere located at the center of the cylinder.

The sizes and relative positions of each sphere are summarized in Table IV.

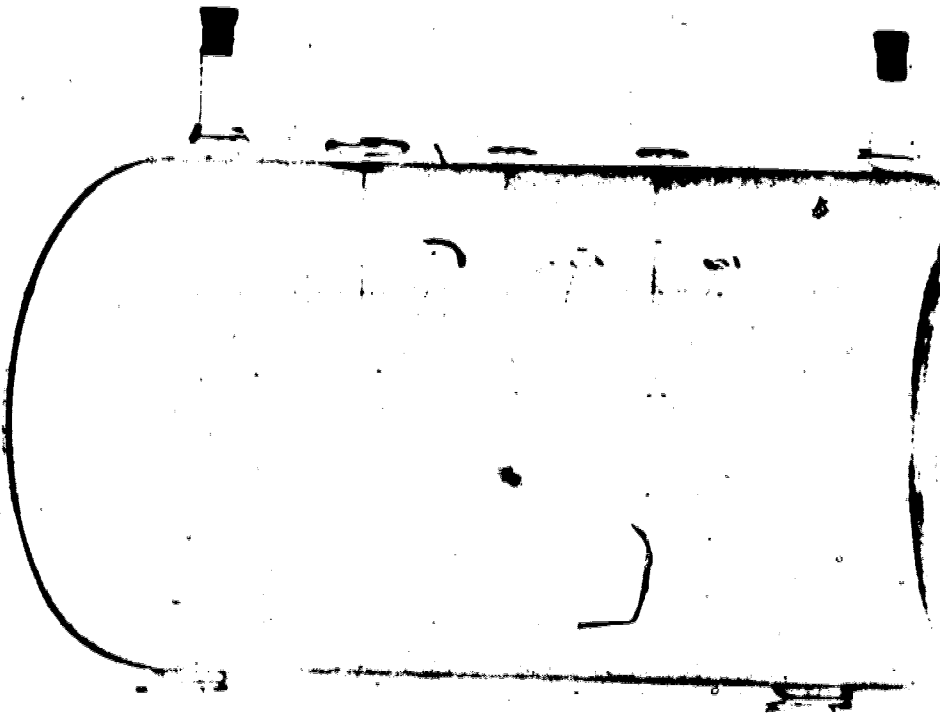


Fig. 8 - 6 l glass phantom with hollow spheres.

TABLE IV

SIZES OF THE SPHERICAL "LESIONS" IN THE GLASS PHANTOM.

	1st Pair	2nd Pair	3rd Pair
Upper Sphere OD	20.0	10.0	10.0
diameter (mm) ID	18.5	8.5	8.5
Lower Sphere OD	10.0	10.0	5.0
diameter (mm) ID	8.5	8.5	3.0

Resolution

On each of the 4 rotating scans carried out on the phantom, the orientation was the same i.e., the cylinder was rotated to position each sphere over its counterpart in the Z plane and the largest (20 mm) sphere located towards the

"base" when viewed in the reconstructed image.

Experiments were carried out to image the spheres both as cold spots on a hot background, and as hot spots on a warm background. In all cases the background material was water and the imaging agent was $^{99m}\text{TcO}_4^-$. The phantom was siliconized to reduce any attraction to the glass surface by the pertechnetate.

For purposes of all calculations, the radioactivity was assumed to be evenly distributed throughout the phantom.

It was realized that the size (or more accurately, the volume) of the spheres was only one consideration in determining the effective contrast between these artificial "lesions" and the background. Perhaps the most significant factor in detecting these abnormalities is the difference in concentration between the balls and the background.

In the run which best illustrated the hot spot to background ratio, the ratio of specific activity was 46:1. The 6.00 l water background had a total activity of 20 MBq. In the reconstructed programme the 20 and all four 10 mm balls were clearly visible; however, the 5 mm ball could not be visually detected.

A summary of the resolution obtained with the different spheres at various spheres to background activity ratios is provided in Table V.

TABLE V

RESOLUTION OF THE SPHERES WITHIN THE PHANTOM AT VARIOUS
SPHERE TO BACKGROUND RATIOS.

Sphere to background Ratio	Spheres Resolved					
	20 mm Static Tomo		10 mm Static Tomo		5 mm Static Tomo	
100:1	-	Yes	-	Yes	-	Yes
62:1	Yes	Yes	Yes	Yes	No	No
46:1	Yes	Yes	Yes	Yes	No	No
27:1	Yes	Yes	No	Yes	No	No
19:1	Yes	Yes	No	No	No	No

One run was carried on the phantom to determine the ability to visually resolve a cold spot on a hot background. In this case, the spheres were left empty and 0.5 GBq of activity was added to the 6.00 l of water in the phantom. The 20 mm sphere was the only sphere resolved in this experiment. The best image of the ball was provided by adding two axial frames. The numerical data (counts per pixel) for a double width horizontal profile through the region of the sphere is shown in Table VI. On this horizontal slice of the axial image, frame # 1 was on the left and frame 64 on the right.

TABLE VI

COUNT DENSITY DATA THROUGH THE COLD 20 mm SPHERE TAKEN FROM
THE RECONSTRUCTED PHANTOM SCAN

Frame Counts		Frame Counts		Frame Counts		Frame Counts	
1	0	17	655	33	319	49	5
2	0	18	650	34	483	50	0
3	0	19	669	35	671	51	0
4	0	20	679	36	735	52	0
5	0	21	668	37	745	53	0
6	0	22	712	38	751	54	0
7	0	23	734	39	751	55	0
8	0	24	665	40	736	56	0
9	0	25	589	41	730	57	0
10	0	26	617	42	792	58	0
11	0	27	690	43	852	59	0
12	0	28	679	44	781	60	0
13	32	29	617	45	596	61	0
14	196	30	570	46	371	62	0
15	417	31	443	47	145	63	0
16	590	32	313	48	12	64	0

Comparison of Regional Count Densities and the Effects of Attenuation

To determine the extent of attenuation within the reconstructed phantom, the axial slices from the previously discussed "hot background" scan were summed through the length of the phantom. Horizontal and vertical profiles 2 pixels wide were taken from these images. Plates 1 and 2 illustrate these profiles, and the numerical count density information is summarized in Table XIV of Appendix 4. This data allows us to calculate the effective count reduction across the cylinder due to attenuation.

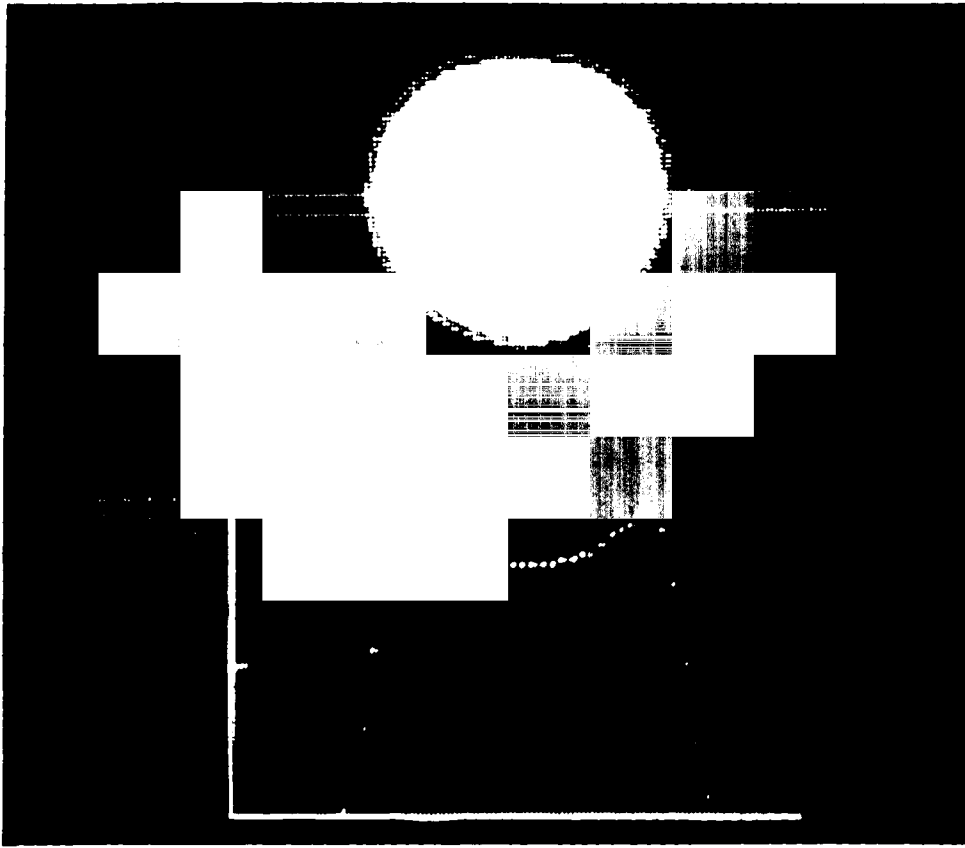


Plate 1 - Distribution of activity across the summed axial planes of the phantom.

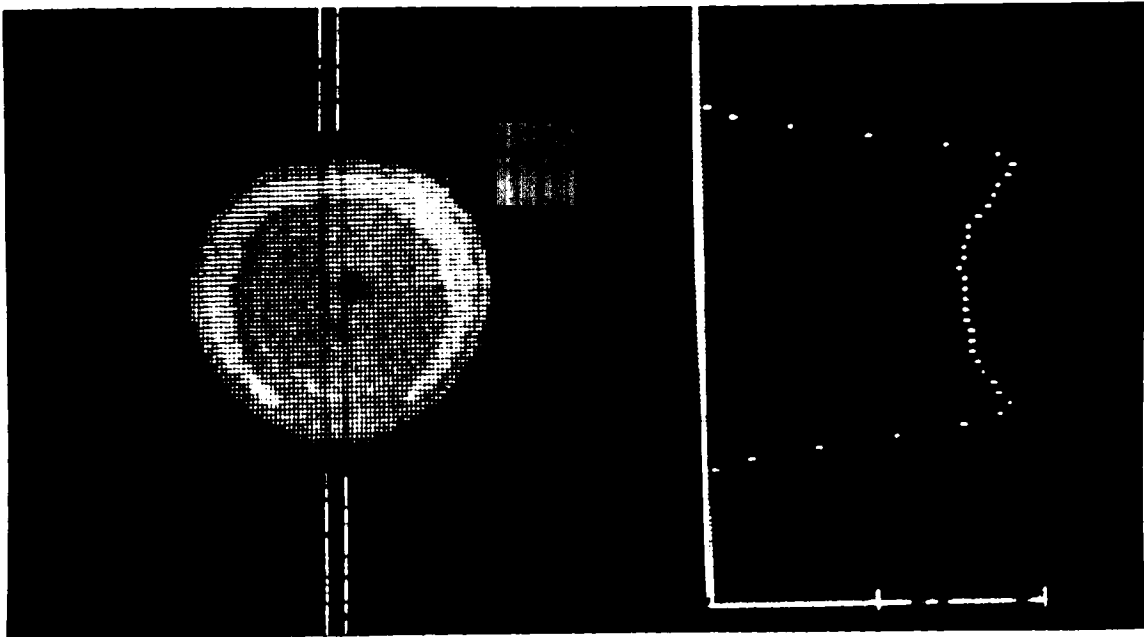


Plate 2 - Distribution of activity down summed axial planes of the phantom.

Expressed as a percentage of the peak count at the edge of the phantom, there is a drop of about 20% at the center of the cylinder. The hammock shape of the curve is characteristic of the influence of attenuation on ECT. The fairly uniform deviation in the central region explains why good images can be obtained without performing corrections for attenuation (82) provided one is working with an approximately cylindrical, homogeneous object.

If we examine the data from the vertical profile, two asymmetries are evident. The height of the phantom taken at half maximum values is 29.5 pixels, down from the horizontal measurement of 31.5. considering the lowest count, 14385, to be the centre of the cylinder, there are 16.0 pixels between the centre and the posterior edge (HM) vs 13.0 pixels from the centre to the anterior edge (measurements are taken from graphs to the nearest half pixel).

The main reason for this discrepancy is that the phantom was filled to a volume of 6.00 l and not to its full capacity. Accordingly, the vertical height should not be the same as the horizontal width. Measurements indicated that the surface was 1.0 cm below the top of the cylinder.

The water level plateau across the top of the cylinder would produce an asymmetry about the horizontal plane of the phantom. Using the observation that there are 16.0 pixels between the centre of the cylinder and the posterior edge, and knowing the internal diameter of the cylinder to be 170 mm (hence a radius of 85 mm), we can calculate that the

reconstructed images provide a relationship which produces a factor of 5.3 mm/pixel in the vertical or Z axis.

In a similar manner, the width at half max taken from the horizontal slice in Appendix 1 has a value of 31.5 pixels. Relating this to the diameter of the cylinder we can calculate that a pixel in the X axis is equivalent to 5.4 mm.

An estimate of the pixel length along the Y axis can be obtained by looking at the number of pixels along the longitudinal axis of the cylinder. Summing the coronal planes and taking a vertical profile down the centre provides the data for Table XVI in Appendix 4. Again using the width at half max values to estimate the boundaries of the phantom, it was determined that 45 pixels corresponded to the 275 mm length. Accordingly, a pixel along the Y axis is equal to 6.1 mm.

In addition to the intrinsic attenuation caused by absorption within the object being imaged, the patient couch further adds to the attenuation component when it is located between the camera and the object being scanned. It is this factor which explains the second non-uniformity observed in the vertical profile of the phantom, i.e. the decrease in the peak edge count on the posterior side of the phantom.

The extent of attenuation caused by the patient couch was calculated by comparing the total counts in the top 3 frames of the rotating scan (63,64 and 1) to the total counts obtained from the bottom frames (31,32 and 33). The

ratio of these counts indicates that the patient bed is responsible for a reduction in counts of 7.5%.

Due to the averaging effect of the tomographic reconstruction, this value will be reduced on the reconstructed image. To calculate the effect of absorption by the bed on the distribution of counts in the reconstructed image, the following method was used. Two square regions of interest (ROI) 16 pixels in area were located anteriorly and posteriorly on axial slices two frames thick. To insure both regions were located at a similar distance from the edge, each ROI was moved 1 pixel up or down to obtain the maximum count rate. This technique insures that any variation was not due to positioning of the regions. It also compensates for any non-uniformity due to camera alignment or positioning of the phantom on the bed. In no case was it necessary to vary the ROI more than 1 pixel unit from its reference location. Table XVII (Appendix 5) summarizes the data obtained from this scan. The last slices at both ends were not included in the tabled information or averaging calculations. The average and SD for the 20 regions in each of the anterior and posterior views is 384 ± 21 and 369 ± 23 respectively. Thus the average reduction in counts in the posterior region of the tomographic scan was approximately 4%, although the large standard deviation negates the significance of this value.

METHOD AND DESCRIPTION OF THE HUMAN TRIALS

The study, divided into two series, consisted of scans carried out on a total of 13 healthy volunteers, 2 of whom were female (DH and LO). Ten of the subjects had never smoked, and of the remaining three, two (DJ and JH) were ex-smokers. LO was a very light smoker of approximately 2 pack-years. None of the group had any respiratory symptoms. The pulmonary function data on the group is summarized in Table XVIII of the appendix, and generally shows normal overall lung function.

The first series of scans was carried out with the subjects lying supine, arms along the side and hands folded across the waist. All rotating scans were taken with the subjects in this position. In the second series, the volunteers had scans done in two positions: supine, with the arms by the sides as in the first series; and supine, with the arms clasped behind the head.

AEROSOL ADMINISTRATION

A schematic of the aerosol delivery system is shown in Fig. 9. The DeVilbiss Model 40 nebulizer is attached to the bag-in-the-box by a short piece of silastic tubing. Two mls. of sulphur colloid labelled with ^{99m}Tc were placed into the nebulizer and the vent was plugged. Compressed air at 30 PSI was used to nebulize the colloid into the bag. The subjects were seated comfortably and placed on the mouthpiece. The 3-way valve was initially set to seal the box and allow the subjects to breathe room air while the nebulizer was generating the aerosol. Aerosol was generated until the volumes of the bag was 6 to 8 l. The compressed air was turned off and the 3-way valve set to permit the subject to breathe from the bag.

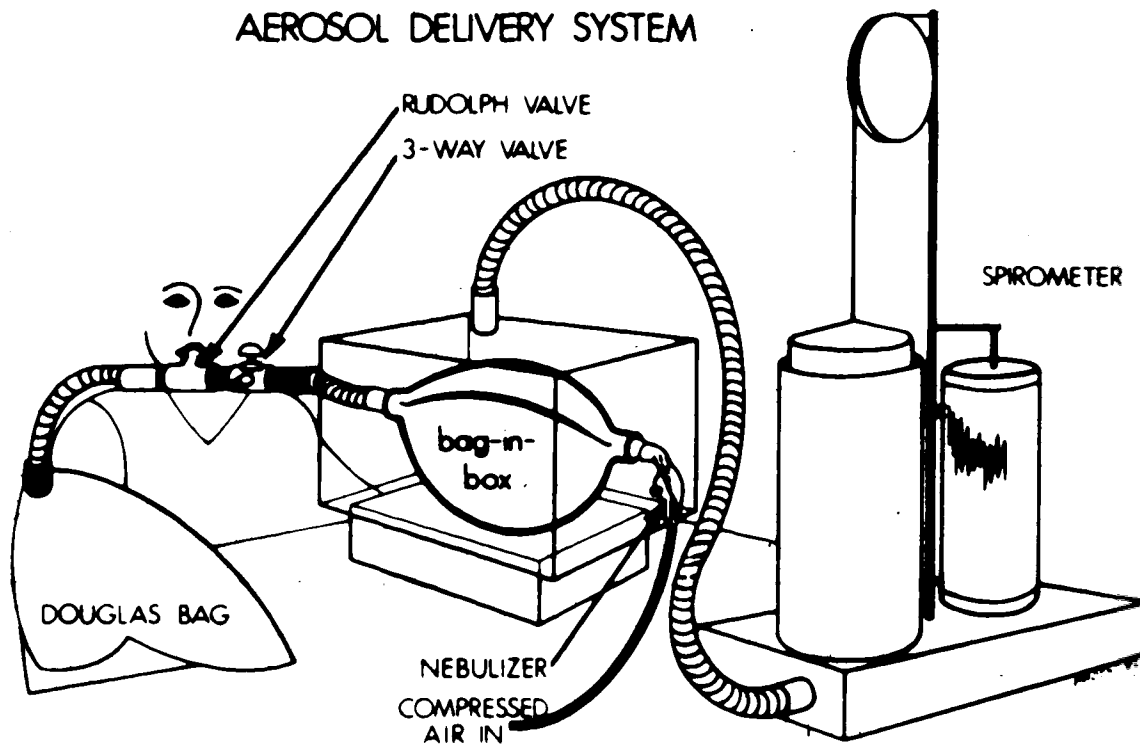


Fig. 9 - Schematic of the Aerosol Delivery System.

The bag-in-box system, first reported by Muir (86), served two purposes. First, it allowed the larger droplets to settle out in the bag thus avoiding more central deposition of these particles in the airways. Second, by connecting the airtight box to a spirometer, it was possible to monitor inspiratory volumes and flow rates during inhalation.

When the bag volume was exhausted, the 3-way valve was again turned to allow the patient to breathe room air while the nebulizer was turned on to fill the bag. This process was repeated about four times or until sufficient activity had been inhaled to provide adequate counts. The subjects were monitored by a Geiger counter during inhalation to provide an estimate of retained activity. Inhalation time was typically in the order of 5 minutes. Following aerosol inhalation, the subjects were taken to the room in which the scanning was carried out.

Ten of the thirteen normals were instructed to inhale from FRC to slightly over tidal volume; the remaining were instructed to breathe somewhat deeper. These latter three subjects were also instructed to hold their breath at the end of inhalation for two seconds. As reported earlier, these two maneuvers should only increase total deposition and have no effect on regional deposition.

RADIOACTIVE LUNG BURDEN DUE TO AEROSOL INHALATION

Direct calculation of the amount of radioactivity retained by the lungs is a difficult task. Simply subtracting the amount remaining in the nebulizer from the initial activity is of course not adequate since some activity is lost to the Douglas bag, the bag-in-the-box, and the tubing. It is not possible to accurately count these losses so an alternate method of calculating the lung burden was used to provide an estimate of the subjects dose.

The technique employed was to compare the count rate observed from injecting a known activity of MAA and comparing this to the count rate observed from the aerosol inhalation. Since the distribution of the two compounds is quite similar, it was felt this was a valid comparison. The intravenous MAA injections were done on two patients who had also received the aerosol. They were seated for posterior static scans. Using a LEAP collimator and a 15% window setting, 37 MBq of injected activity corresponded to 3,070 cps \pm 220 counts. The range of count rates observed in all of the aerosol trials was from 460 to 4600 cps with mean and standard deviation of 2,480 \pm 1,300 cps. The calculation then indicates a mean burden delivered to the patient of 30 MBq.

Using the MIRD (87) tables and assuming no clearance of particles from the lung, the maximum radiation dose to the lungs from the aerosol is 0.12 mGy/MBq, or 3.6 mGy for the average dose to a patient in the series. The maximum dose

to the subject who had a 1 sec. count of 4600 would be 6.7 mGy. This value is comparable to the lung burden for the standard injection of 110 MBq of MAA for a perfusion lung scan which exposes the lungs to 6.3 mGy (88). If the aerosol were given to patients with COPD, considerable clearance would normally be noticed and the lung burden due to the aerosol exposure would be reduced; however, the dose to the tracheal epithelium and GI tract would correspondingly rise.

QUALITY CONTROL IN THE RADIOCOLLOID PREPARATIONS

The technetium labelled sulphur colloid preparations were reported by the Edmonton Radio Pharmaceutical Centre (85) to contain 5% or less free pertechnetate on those days in which our experiments were carried out. Some samples were taken of the sulphur colloid after nebulization from both the bulk solution remaining in the nebulizer, as well as from the plates in the cascade impactor. The impactor samples were redissolved in saline and analysis by thin layer chromatography (GELMAN ITLC-SG) was carried out. Analysis of the strips was done on a Canberra Series 40 multi-channel analyzer (Canberra Industries Inc., Meriden, Connecticut) connected to a Berthold model LB 2832 automatic TLC linear analyzer (Berthold, Wildbad, W. Germany). In one test carried out, all samples, both in the original preparation and diluted samples, yielded less than 3% free pertechnetate. This applied to samples tested both before and after nebulization.

The addition of albumin appeared to absorb any free TcO_4^- remaining in the sulphur colloid preparations, despite the fact that no tin was used in the manufacture of the colloid. No solvent front activity could be distinguished in those solutions to which albumin had been added, indicating a binding efficiency close to 100%. The binding of the TcO_4^- to the albumin is unlikely to be as strong though as the Tc-sulphur colloid complex or even standard

Tc-HSA preparations, due to the absence of the tin.

The low level of free pertechnetate in the original colloid solutions in conjunction with the stability of the nebulized compounds combine to make ^{99m}Tc sulphur colloid a suitable agent for short term radioaerosol lung imaging.

LUNG IMAGING AND TOMOGRAPHIC RECONSTRUCTION

The camera system used for imaging was the 400T version of the G.E. Maxicamera II. Most tomographic images were obtained by acquiring 64 frames on the rotational scan. The time per frame varied from 27 to 47 seconds depending upon the amount of activity present in the lungs at the time of the scan. The gamma camera was fitted with a low energy high resolution parallel hole collimator and a 15% energy window was centered at the photopeak.

During tomographic scanning, data was acquired on a PDP 11/34 computer using a specially written program. Tomographic reconstruction was carried out on a PDP 11/70 computer connected via a Decnet link to the 11/34. Reconstruction was done simultaneous with data acquisition and image reconstruction was completed by the 11/70 within 2 1/2 minutes of data acquisition. The reconstructed images were then transferred back to the 11/34 for display and analysis using both GAMMA-11 software and special user written programmes. Permanent copies of all scans were stored on magnetic tape for future reference.

DATA ANALYSIS AND RESULTS IN THE HUMAN TRIAL SERIES 1

Of the 10 normal subjects in the first experimental study, 9 tomographic reconstructions of aerosol deposition in the lung were suitable for analysis. Subject, KM, was lost to the study due to inadequate nebulization of the aerosol and the resultant small amounts of activity in the lungs. This was due to an exceptionally "sticky" batch of colloid which yielded a low activity output efficiency, (~1%) from the nebulizer. (It was the result of this experiment which led to the use of albumin in the nebulizer solution. As mentioned earlier, this increased the activity output efficiency of the colloid to about 30%).

Several methods of analysis were considered for determination of the regional distribution of radioactivity in the lung. The first technique chosen involved the use of the sagittal planes in the reconstruction. For each lung, the sagittal frames were added together and analysis was carried out by dividing the lung into four approximately equal quadrants. The average count densities (average counts per pixel) in each of the four regions were calculated by the Gamma-11 programme. Plate 3 illustrates the division of the LL into quadrants on subject JH.

This procedure was followed for all subjects. The average counts per cell were then expressed as a percentage for the lung (left or right) and this percentage was averaged for all the subjects to provide the data for Table VII. For the reasons presented in the discussion, this

approach was found inadequate in describing the distribution of activity within the lung. By coincidence, however, it does show the trend which was found to occur by another analytical method.

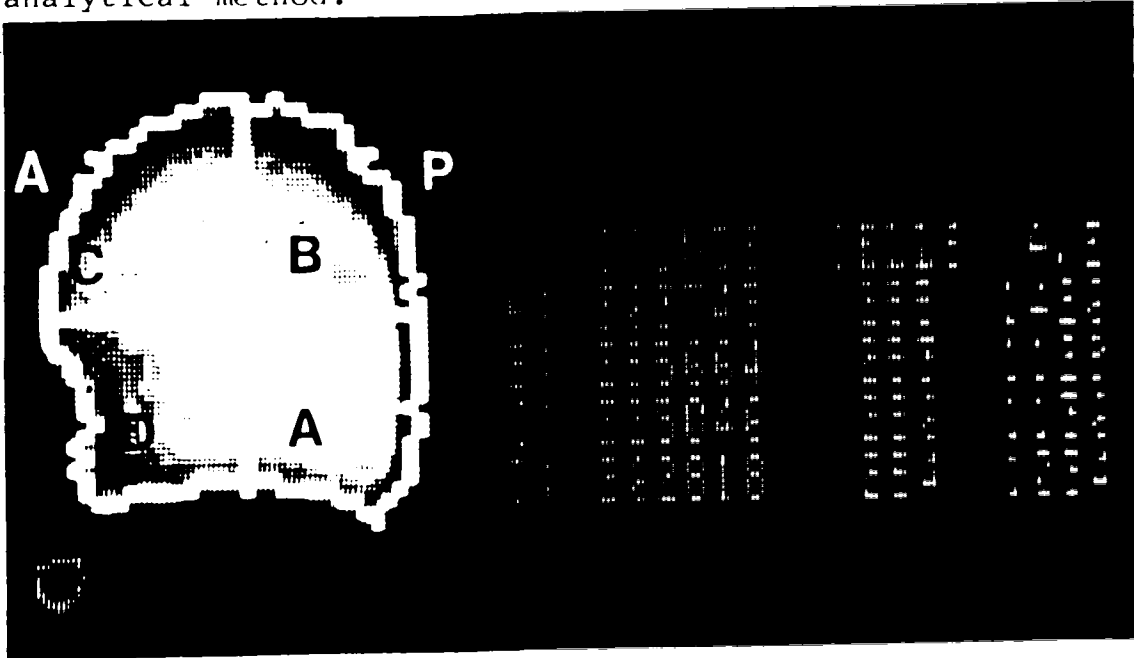


Plate 3 - Division of the left lung of subject JH into quadrants to illustrate regional count variations.

TABLE VII

THE DISTRIBUTION OF ACTIVITY IN A DEFINED GRADIENT OF THE LUNG EXPRESSED AS A PERCENTAGE OF TOTAL LUNG ACTIVITY

Region	Regional % of Total Left Lung	Intersubject Standard Deviation	Regional % of Total Right Lung	Intersubject Standard Deviation
A	32.1	2.6	29.7	2.4
B	25.4	1.5	24.6	1.4
C	22.3	1.9	22.5	1.3
D	20.1	1.9	23.2	2.1

In choosing an alternate method of analysis, several factors would have to be considered. The ideal system would permit a true count per unit volume (count per unit voxel) and, if a valid comparison were to be made between two regions, the method would have to maintain some form of symmetry to ensure minimal attenuation error. It would also be desirable to avoid the outer regions of the lung which present difficulties in defining the lung margins, mainly due to the regional variations in movement which occur during the scan.

The method of analysis chosen which best fits the required criteria involved the use of two regions of interest (ROI's), 4 pixels on a side placed over the anterior and posterior regions of axial frames of each lung. They were positioned so that they were at the edge of the lung but contained an area which was unequivocally within the lung. In addition, the axial slices were grouped in units of two to yield a volume of 32 voxels or, based on earlier calculations, 5.6 cm^2 per dual frame.

By redrawing the ROI's on each successive pair of axial slices, it was possible to maintain regions consistent with a relative position in the lung from the base to the apex and, at the same time, maintain a symmetry with respect to the lung tissue. The choice of anterior and posterior regions also reduced the chance of including airways or major blood vessels within the ROI. Plate 4 illustrates the positioning of these regions in lower and upper axial slices of the lung (subjects LO and KH respectively).

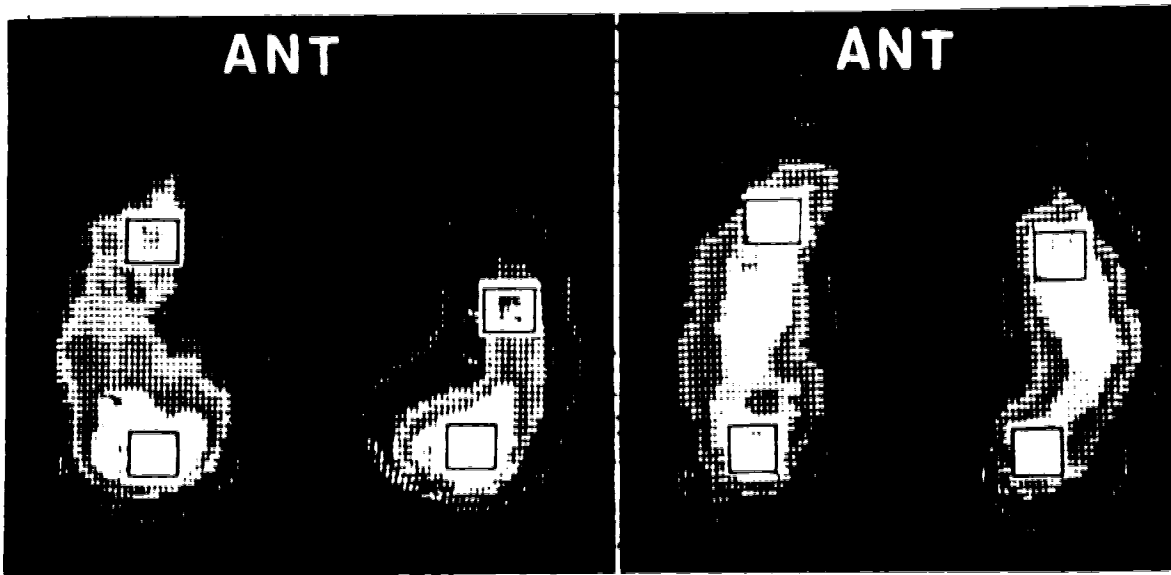


Plate 4 - Positions of the ROI in the lower (left) and upper (right) sections of axial slices of the lung.

The data obtained using this method on subject MY is illustrated in Table VIII. In the axial planes, the frame numbers refer to the Y axis of the reconstruction with the lower frame numbers representing the base of the lung. The anterior counts start at a higher frame number due to the shape of the lungs.

It should be pointed out that the numbers obtained do not represent absolute counts. During the reconstruction, the pixel which contains the highest count is scaled down to the maximum value of 255. All other cells are then scaled down by a similar ratio to maintain linearity. In calculating the expected variance for a series of regions, using the observed numerical values would lead to an overestimate of the variance. As the true variance is not only

a function of the absolute counts used in the reconstruction but other factors such as signal to noise and filtering functions, the variance chosen for analytical comparisons was based on the numerical values obtained from the trial.

TABLE VIII

COUNTS (ARBITRARY UNITS) OF ANTERIOR AND
ROI FROM AXIAL FRAMES OF SUBJECT

Frame Number	Right Lung		Left Lung	
	Anterior	Posterior	Anterior	Posterior
86		112		161
88		208		282
90		303	183	348
92		353	259	437
94	248	358	254	296
96	276	336	240	355
98	244	327	233	245
100	252	333	261	340
102	259	312	278	346
104	259	302	280	350
106	271	269	288	338
108	291	273	315	310
110	290	281	290	331
112	300	261	257	267
114	281	241	239	228
116	212	209	195	195

It may be recalled that the average anterior and posterior ROI's from the axial slices had values of 384 and 369 with respective standard deviations of 21 and 23. The coefficient of variation for these two values are 5.5 and 6.2%. Based on this data, the best variability that could be expected in a completely uniform distribution would have approximately this coefficient of variation. To insure that any conclusions would not be over-biased to favour the experiment, the coefficient of variation was set at 7% for all calculations.

Two interesting factors emerged from the analysis. Most striking was the observation that in roughly the lower half of the lung there was a marked difference in deposition of the aerosol between anterior and posterior regions. A similar pattern was noticed in both lungs. Of the 9 scans analyzed (and no attenuation correction applied to the posterior region to correct for the patient couch), a difference significant at the 5% level was noted in all cases except one (HY, right lung only). The levels of significance for each patient are tabulated in Table IX. Incorporating the 4% attenuation correction to the posterior region would increase the level of significance to 1% in most cases.

TABLE IX

LEVELS OF SIGNIFICANCE BETWEEN ANTERIOR AND POSTERIOR ROI
IN THE LOWER AREAS OF THE LUNG

Subject	Left Lung Level of Significance (%)	Right Lung Level of Significance (%)
PM	0.01	2.0
MY	0.1	0.01
HY	0.1	10.0
DR	0.1	0.1
KH	0.5	2.0
DH	<0.1	5.0
DJ	0.1	0.2
LO	0.1	0.001
JH	5.0	0.1

Based on a proportion of counts between the posterior ROI to the anterior ROI in those frames with significant differences (in the lower portion of the lung), the posterior region had an average of 45% higher activity in the left lung and an average of 38% higher in the right. If an attenuation correction for the patient bed was applied to the posterior regions, these values would rise even further. Plate 5 illustrates the regional count density gradient in an axial slice (dual frame) of the lower right lung of subject DJ.

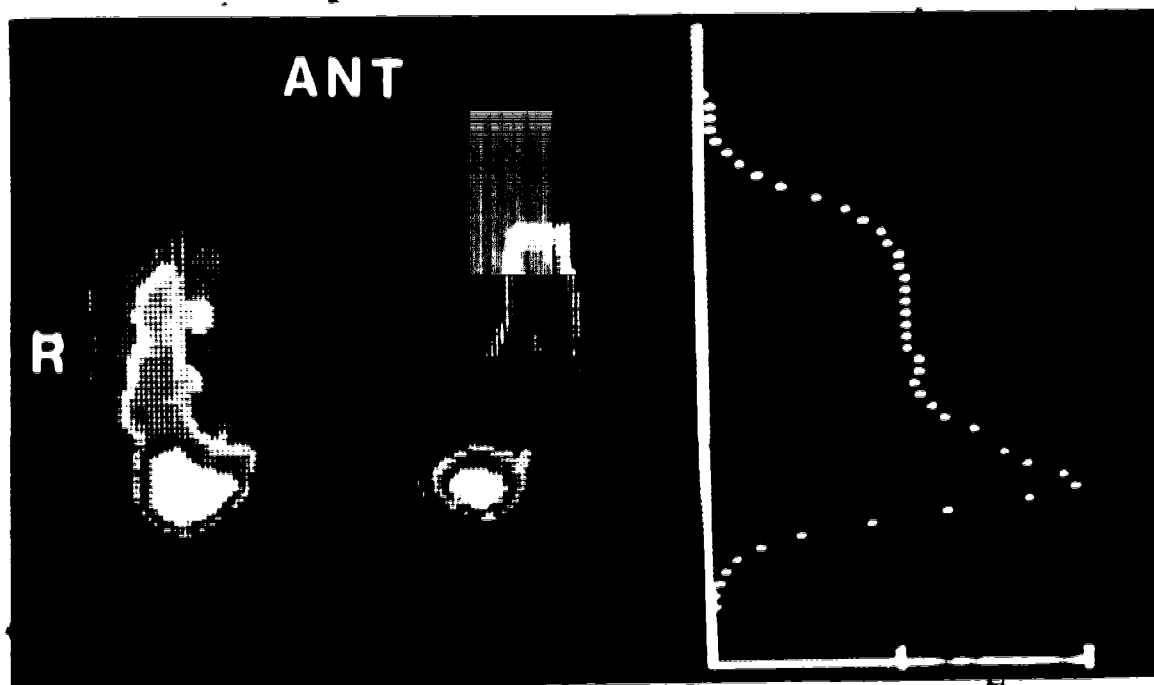


Plate 5 - Count distribution through an axial slice (dual frame) of the lower right lung of subject DJ to show regional variations.

The lower anterior region was only paired to its posterior counterpart if it fell within 1 standard deviation of the average of the next 4 anterior frames. The upper half (roughly) of the lungs were analyzed in a similar manner. In contrast to the lower regions, the upper areas did not show significance at the 5% confidence level between anterior and posterior ROI in any subject. For each individual, this horizontal gradient dropped off rapidly in the central region of the lung, suggesting that the differences were possibly due to lobar or segmental variations in regional deposition. These results imply that

activity must be evenly distributed on a horizontal plane in the upper regions of the lung.

The second important finding which can be determined from the data reflects the distribution of the aerosol in the vertical gradient of the anterior portion of the lungs. It was found that there was no significant difference (at the 5% level) in any subject in the variation of regional counts between the base and apex in the anterior ROI of the lungs. The average variability in the counts for the population produced a standard deviation of 1.2 in the left lung and 1.1 in the right. These values are again based on the assumption of a coefficient of variation of 7%.

One difficulty experienced in the analysis was deciding the edge of the lung. The process is made difficult by the fact that the lung moves during scanning. Although the positioning of the ROI at a level well inside the lung eliminates most of the problem, there is still some uncertainty at the apical and basal regions. As the average counts for a ROI begin to drop at these extremes, one must decide whether this is due to a biological decrease in activity, attenuation, lung movement during the scan or the fact that the axial slice is actually leaving the region of the lung. Undoubtedly, all of these variables are probably occurring to some degree. The problem, however, mainly occurs at the top 2 or 3 cm of the lung and any vertical gradient which may exist should be detected before this height.

Accordingly, to establish a consistent pattern for analysis, a pair of frames was only included in the average provided it fell within 2 standard deviations of the average of the central frames. For example, in Table VIII the average of the anterior ROI between frames 92 and 114 (inclusive) in the left lung was 266 with a standard deviation of 24.5. Thus the top and bottom frames would have to exceed $266 - 49$ or 217 counts to have been included in the analysis.

The significance of these findings is presented in the discussion.

DATA ANALYSIS AND RESULTS IN THE HUMAN TRIAL SERIES 2

The purpose of the second experimental series was to determine the effect and degree of attenuation caused by the arms on the reconstructed lung images. Five scans were obtained with the hands clasped behind the head, thus eliminating the arms from the field of view of the camera. In four of these five experiments rotating scans were also obtained with the arms along the side (as in the first series) to provide data for which a comparison could be made between the two procedures. Two subjects (JH and KH) from the first series returned for this second scan and were joined by three new subjects (WL, CM, CC).

Analysis was carried out using the $4 \times 4 \times 2$ voxel ROI superimposed on axial slices as was utilized in the first experimental series. Again, with the arms by the side, a significant difference (at the 5% level) existed between anterior and posterior regions in the lower lung zones of all subjects and no significant horizontal gradient was found in the upper portions of the lungs.

The results of the scans with the arms behind the head did, unfortunately, not provide conclusive data. Two of the five subjects still demonstrated a significant horizontal difference between the anterior-posterior regions in the lower lungs; the remaining 3 did not. Once again no significance was noted in the upper portion of the lung for the paired regions on any individual. Even if a 4% attenuation correction for the patient bed was applied to

the lower posterior ROI, the numerical values obtained still did not demonstrate a significant difference between the two regions in any of the three subjects.

It can be pointed out, however, that there was still a trend for the lower posterior region to be higher in activity. In these three subjects, the posterior ROI was still an average of 9% higher in counts than the anterior region (attenuation corrections would increase this value even more). In addition, the "hottest" ROI's were always located posteriorly. The overall increase of activity in the lower posterior regions for the five subjects who were scanned with arms behind the head, averaged $20\% \pm 18\%$ (range 3.2 to 62.1%) compared to the average of $42\% \pm 13\%$ (range 20.6 to 76.6%) for the subjects in the first series.

A COMPARISON BETWEEN REGIONAL BLOOD PERFUSION AND
AEROSOL DEPOSITION

Two of the twelve subjects (JH and LO) in the aerosol trial were also given ^{99m}Tc MAA injections, followed by tomographic scans. One other subject (KM) not included in the aerosol trial also received the injection. MAA was administered intravenously to the forearm in the conventional manner except that the subjects were seated during the injection. The rotational scans were carried out using the same protocol as was used in the first aerosol study (with the arms by the sides.) Instrument settings were identical with the possible exception being that the time per frame and reconstruction filter intensity were adjusted to optimum conditions. Between 40 and 60 mBq of activity was injected, roughly half of the dose normally given to a patient in perfusion scans.

Analysis was once again carried out using the 16 pixel ROI areas located at anterior and posterior edges of the lung on the axial frames. Again the increase in activity was noted in the posterior region of the lower lung relative to the anterior region at the same level. In five of the six cases this difference was highly significant (0.5%). As with the aerosol, this significance disappeared in the upper lung zones.

In these runs both the anterior and posterior regions dropped in counts towards the apex demonstrating the vertical gradient due to hydrostatic pressure.

TABLE X

A COMPARISON OF THE DISTRIBUTION OF
 ^{99m}Tc MAA (PERFUSION) AND ^{99m}Tc SULPHUR COLLOID
 AEROSOL IN THE RIGHT LUNG OF SUBJECT LO

Frame	PERFUSION		Signif- icance % Level	AEROSOL		
	Anterior ROI	Posterior ROI		Anterior ROI	Posterior ROI	Signif- icance % Level
84		188			231	
86		329			375	
88		401			414	
90		427			389	
92	274	443	<.05	203	363	<.05
94	312	418	.5	228	325	.1
96	287	390	.5	211	317	.01
98	274	365	.5	194	308	.01
100	245	340	.5	191	313	.01
102	243	329	.5	193	313	.01
104	240	267	N.S.	233	268	N.S.
106	230	217	N.S.	249	231	N.S.
108	195	171	N.S.	250	243	N.S.
110	142	129	N.S.	230	206	N.S.
112	89	85	N.S.	162	156	N.S.

This information can be displayed numerically as shown in Table X which compares the perfusion and aerosol scans for the right lung of subject LO. The significance level of each anterior - posterior pair is also indicated. Again the level used to determine significance is .05.

In this specific case the ratio of the posterior to anterior counts in the perfusion scan for the lower lung indicates a 35% higher blood flow to the posterior region while the aerosol scan shows a 59% increase in the same area. Similar results were obtained for the subject's left lung and in the other two subjects. The average difference in the lower regions of the lungs in the three subjects indicated a 34% higher blood flow to the posterior region.

CHAPTER IV

DISCUSSION

PHANTOM MEASUREMENTS

The data provided by the tomographic scans of the phantom confirm the basic technique of tomographic reconstruction. The analysis is limited, however, in that the phantom is symmetric in shape and has an even distribution of activity. In addition, it was filled with water with a density of 1.0. Lungs, on the other hand, have a density about 1/3 that value. Accordingly, attenuation in the lung area would be considerably less than observed in the phantom over the same distances.

Tomographic analysis of the artificial "lesions" demonstrate that small abnormalities can be detected, even at a considerable depth. The 5 mm hot sphere was not visible on the run when the concentration ratio for hot spot to background was 62:1. The volume contained in this sphere is 0.014 cm^3 , one twenty-third that of the 10 mm ball. Accordingly, the activity contained in that volume was only $0.08 \text{ } \mu\text{Ci}$ (vs $1.9 \text{ } \mu\text{Ci}$ for the 10 mm and $18 \text{ } \mu\text{Ci}$ for the 20 mm spheres) hardly enough to image at the best of times even in air. Given the scan time of 22 seconds per image, the collimator resolution and the depth of the ball in the water, it is not surprising that the 5 mm sphere could not be resolved under the above experimental conditions.

A similar argument applies to the imaging of the 20 mm sphere as a cold spot in a hot background. As it is located at the center of the cylinder, it is effectively masked by 80 mm or so of water.

Thus the phantom trials verified the ability of the technique to delineate 2 cm abnormalities at a depth of 8 cm in water (or tissue of similar density).

Phantom measurements also provided an indication of the nature and extent of attenuation on the reconstructed images; attenuation caused both by the imaging medium as well as external factors such as the patient couch.

Of the two methods used to measure the attenuation by the patient bed, the most valid is probably the average of the 3 anterior frames in relation to the average of the 3 posterior frames. This measured value of 7.5% corresponds to the published figure of 8% for attenuation by the bed for 140 keV photons (82). The current reconstruction program has no attenuation correction factors built in. It has been suggested that, as a first step, this factor of 8% be added on to regions in those frames in which activity must pass through the bed to the camera. The result would be to produce a more uniform image of the phantom and a truer distribution of activity in the patient studies, especially in the posterior regions of the image.

The "hammock" shape distribution of attenuation with depth as illustrated in Plates 1 and 2 actually benefits the study of human organs by providing images of high quality without any attenuation corrections applied to the program. If we assume a chest wall thickness of 2 cm (about 4 pixels) and a density of the tissue in the chest wall of 1.0 we can see that the areas of greatest change, i.e., the

edge of the phantom, will be eliminated. An estimate of the change in attenuation over the next 7 cm of water (or 21 cm of lung tissue) would amount to about 10%.

THE HUMAN TRIAL

In addition to the intrinsic attenuation of the gamma particles described in the phantom trial, scanning human subjects introduces additional problems. Specifically, the effects of the arms, the heart, and the chest wall will all create some artifacts in the reconstructed images. Of the three, the arms are suspected of having the most significant influence on the reconstruction.

Despite the variable effects of the arms noted on the scans in the second series of experiments, the data still indicates an increase in activity to the lower posterior regions of the lungs.

It is not entirely clear how one may relate these observations to lung anatomy and physiology. It can be seen in Plate 5 that the gradient between anterior and posterior regions is not a smooth change, but rather occurs in the posterior third of the lung only. Based on observations of the location of this "hot" region in all subjects, the initial conclusion was that the regional increase in deposition was a function of lobar or, more probably, segmental variations in deposition within the lung. Specifically it is suggested that the apical and posterior basal segments of the lower lobe in the left and right lungs receive the greatest deposition of $1 \mu\text{m}$ particles per unit volume within the lung. The remainder of the lung receives a lower but evenly distributed density of aerosol deposition. Although this is a new finding in humans, it

would seem to receive support from the observations of the animal experiments discussed in the literature survey (11-13).

One possible explanation for this increase could be that the anatomical structure of the airways is different in this region compared to other areas of the lung. These variations may be due to an increase in the bifurcation angles in the lower generation of the airways of this region or possibly due to an increase in the relative length of the airways.

Series 1, Sagittal Analysis

The method of analysis carried out by dividing each lung into four quadrants has several limitations despite the fact that it does provide some useful information.

The major limitation in this analytical technique is that it does not portray a true count density. While it accurately reflects the counts within the volume of each ROI, it does not take into consideration that the lung volume within each quadrant in the depth (X) direction may not be the same. For example, if the lungs were to have a uniform distribution of radioactivity throughout but be wider at the back than the front, the posterior regions would show larger average counts per pixel on the summed regions used to outline the lung. While the thresholding technique reduces this error somewhat, both inter and intrasubject variability of the regions will be increased

making it more difficult to decide on any significant differences which may occur.

It can be seen from Table VII, which illustrates the 4 lung quadrants, that there is roughly a 50% difference in the average counts per voxel between regions A (lower posterior) and D (lower anterior). To properly analyze the significance of this difference we have to include both the intersubject variability as reflected by the standard deviations in Table VII, as well as determine an estimate of the intrasubject variability.

The latter was done by measuring the results of two subjects, each of who received 4 tomographic scans after their inhalation. It was assumed that, once deposited, the aerosol did not significantly change its distribution during the interval between the first and last scans. The four regions, once chosen, were superimposed on scans to avoid any bias due to redrawing of the areas. The variation in the average counts per pixel for each of the regions was then calculated for the two subjects. These values were averaged to provide an estimate of the intrasubject variability. This value, which under ideal conditions should be 0, was found to be roughly 3% (each region, in fact, was given its respective percentage).

When inter and intrasubject variances were added together, it was found that only 2 pairs of the 8 regions showed any significant differences. These regions were the A and D areas in the left lung and the A and C (upper

anterior) areas, also in the left lung. The levels of significance were 1 and 2% respectively. Regions A, C, and D in the left lung had no significant differences (at the 5% level) from each other and none of the regions in the right lung showed any significant difference at the 5% level to any other region.

The second limitation with this method of analysis is that the division of the lung into quadrants does not reflect the true anatomical divisions found within the lung, i.e.; region B, the upper posterior quadrant, would include both upper and lower lobes. It may, in fact, be a difficult task in any analytical method to determine specific segments or lobes within the lung as there are no distinguishable anatomical markers visible in the reconstructions. In addition, the Gamma 11 programme is not able to rotate the tomographic images to allow planes to be drawn which would correspond to the angles of the segmental divisions between inferior and superior lobes of the lung.

Anterior-Posterior ROI Comparison

The reasons for, and advantages of this method in the analysis of the deposition were previously discussed. The major advantage of this technique over the sagittal quadrant analysis is that the ROI's can provide a true count density approximation for the region of lung in which they are located. It can be pointed out that the size of the regional volume (4x4x2 pixels) was chosen for practical

reasons. A larger ROI would, in some cases, necessitate regions on or outside the lung margin, thus giving the appearance of a lower count density than may actually occur within the lung. On the other hand, choosing a smaller region would create lower numerical values, hence increasing the statistical error.

It may be recalled that subject-HY did not demonstrate a significant difference between the anterior and posterior regions of his right lung. The lack of significance in this case may be due to the shape of this individual's lungs rather than to some lack of consistency between the anterior-posterior gradient noted in the other subjects. HY appeared to have a liver which rested considerably higher than normal under his right lung. In fact only one anterior ROI could be drawn in his right lung before the mid height of the lung was reached. Accordingly, the horizontal gradient for this lung could only be based on a comparison in this one frame. In most subjects at least 5 frames were usually used to establish a level of significance between anterior and posterior regions in both the upper and lower lung regions (see Tables VIII and X). Thus, the difference observed in HY may be due to a structural variation rather than a true aerosol distribution deviation from the observed trend.

As noted earlier, the lower posterior regions of the lung appeared to receive a higher concentration of the $1 \mu\text{m}$ aerosol. While there was evidently a vertical gradient

in the posterior ROI, there was none in the anterior portion of the lung. The conclusion reached here was that the overall vertical gradient seen in static scans was due solely to the posterior gradient. (It must be remembered that the vertical gradient seen on static scans is due, in part, to the fact that the lungs are wider at the base than at the apex - hence there will be more activity "seen" by the camera in this lower region of the 2-dimensional static scan).

An approach which would tend to confirm the tomographic findings would be analysis of anterior and posterior static scans. The fact that 2 dimensional static scans reflect attenuated activity through the lung is actually beneficial in this comparison for while it averages activity throughout the depth of the lung, the activity in the region closest to the camera will dominate the image. Accordingly, if an anterior vertical gradient didn't exist and a posterior vertical gradient did, the net gradient would be more noticeable on posterior scans.

This was indeed the case on the one subject, JH, who received static anterior and posterior scans. The results of vertical slices through the right lung of these two images are illustrated in Plate 6 and the numerical counts are tabled in Appendix 7. A plot of these values over the top 2/3 of the lung yields a slope of -39 for the anterior scan and -80 for the posterior scan.

It is suggested that, in fact, most of the "vertical

gradient" seen on the tomographic scan is due to the higher count density on the lower posterior region of the lung and not to the fact that the lung is wider at the base than the apex. The end effect is to create an apparent illusion of an overall decrease in count densities as one goes up the lung. This analytical approach confirms the findings of the tomographic reconstruction.

While the attenuation caused by the arms was known to affect the reconstruction it was felt that it should have a minimal effect on the ROI's for the following reasons:

- 1) There was no visible evidence of an arm "shadow" on the reconstructed lung images;

- 2) The arms were positioned parallel to the body. Accordingly it was felt that any effect they would have on the ROI would act equally on both anterior and posterior portions of the body; and

- 3) The nature of the reconstruction is such that there is an averaging effect of the 64 frames on any attenuating regions between the lungs and the camera. Thus, the absorbance caused by tissue external to lung activity would be distributed over a wider range. This would in turn reduce the effect on lung tissue immediately posterior to the attenuating factor (in this case, the arms).

The reason for 2 of the 4 individuals to change so markedly in their reconstruction scans after moving their arms out of the view of the camera, and the others not, is unclear. It may relate to the shape of the chest or to the

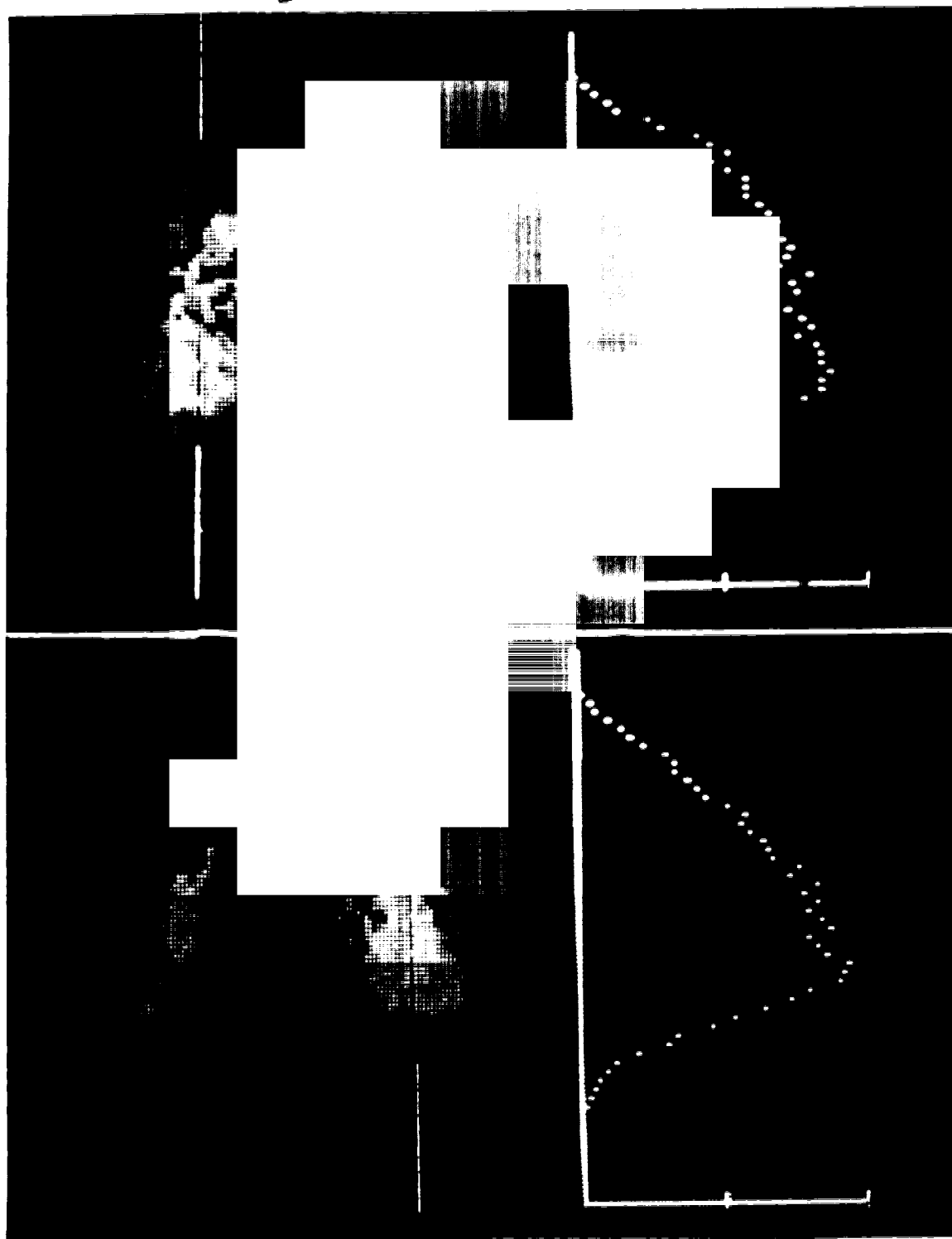


Plate 6 - Vertical slice profiles through the right anterior (top) and posterior (bottom) static lung images of subject JH to show distribution variations.

exact position of the arms during the scan. It is possible that some individuals have a deeper chest, and the arms, though parallel to the body, were actually positioned quite anterior relative to the lungs. Larger arms would attenuate the gamma photons to a greater extent than smaller ones. While no measurements of chest or arm size were taken, the build of the 5 males in this study was quite similar with the major variation perhaps being in height.

As previously mentioned the tomographic perfusion scans indicated a 34% higher blood flow to the posterior lung region relative to the anterior region at same height; a value somewhat less than the 42% figure found in the first aerosol series. The literature does not appear to quantitatively discuss blood flow per unit lung volume in the human. It may turn out to be that the apical and posterior basal segments of the inferior lobes not only receive a relative increase in aerosol and blood flow, but are better ventilated as well.

CHAPTER V

CONCLUSION

The studies undertaken for this thesis have provided an insight into the generation and behavior of aerosols, as well as supplying new information on particle deposition in the human lung. Additionally the research has posed new and challenging problems.

The aerosol of ^{99m}Tc sulphur colloid has proven to be satisfactory as a lung imaging agent. Its in vivo stability provided consistent and reproducible measurements of lung retention for up to 24 hours, which was not possible with ^{99m}Tc labelled albumin aerosols. Accordingly, sulphur colloid solutions stabilized with HSA are recommended for studies of aerosol deposition in the lung. It remains to be seen whether or not a technique for generating larger droplets of colloid suspensions can be developed to permit the study of particle deposition of 3 to 10 micron aerosols.

The aerosol delivery system was also found to perform adequately in generating the $1\ \mu\text{m}$ aerosol. Some modifications could be made to the apparatus. Such items as shielding for the nebulizer and Douglas bag which would reduce radiation exposure to the technicians and patients, a more integrated and adjustable valve and mouthpiece arrangement, and better air pressure/regulator systems for the nebulization process would all improve the technical design of the system.

SPECT carried out on normal subjects led to the following observations:

- 1) Tomography can provide a 3 dimensional visual display of lungs imaged with radiolabelled aerosols.
- 2) We may obtain count per unit volume information without using ^{133}Xe to estimate lung volumes.
- 3) Attenuation artifacts caused by the patient couch, or more physiologic causes such as the patients arms, can have a marked effect on the quantitative results of the reconstructed scans.
- 4) The apical and posterior basal segments of the lower lobes receive a higher deposition of $1\ \mu\text{m}$ aerosol than do other regions of the lung. This increase was also noted in the MAA blood perfusion studies.

In order to confirm the findings presented, the reconstruction programme should be modified to include attenuation corrections. Ideally, a transmission system should be developed which would provide measurement of individual chest densities. This information could then be applied in the form of an attenuation correction to the emission data. One suggestion put forward has been the use of a transmission flood plate parallel to the gamma camera on the opposite side of the patient. This system would create a form of CT image. If the energy of the isotope used in the plate were sufficiently different from that of $^{99\text{m}}\text{Tc}$, and a dual synchronous isotope mode incorporated into the camera, both scans could be carried out at the same

time. The information from such a dual scan would be subject specific and eliminate the problem of repositioning the subjects for a subsequent scan.

Research into lung deposition of aerosols should continue. In the meantime, it is imperative that a protocol be established to handle the positioning of the arms away from the view of the gamma camera. When possible, this can be done by clasping the hands behind the head. Other approaches may be to extend the bed and provide a support for the arms above the subject's head. It may even be possible to reverse the position of the patients on the bed so the feet are towards the counterbalance of the camera.

Once the problem of attenuation has been adequately dealt with, there are several areas which deserve further investigation using the tomographic technique. Briefly, these are:

- 1) confirmation and quantification of regional deposition of $1 \mu\text{m}$ aerosols
- 2) a more thorough investigation of the distribution of blood flow in the lungs using $^{99\text{m}}\text{Tc}$ MAA
- 3) a comparison between blood flow and ventilation, preferably using a higher energy radioactive gas than ^{133}Xe , such as ^{81}Kr
- 4) studies of aerosol deposition using larger particles. These investigations would provide information concerning both regional clearance and regional deposition. If the observations

made in this thesis are confirmed, it would be worthwhile to determine if the increased regional deposition in the lung is a function of particle size.

The potential role of single photon emission computed tomography as a tool in lung imaging has been demonstrated. With improvements in the reconstruction programmes, SPECT will greatly aid to our understanding of the behavior of inhaled particles as well as regional blood flow patterns and related lung physiology.

REFERENCES

1. FIRST, M.W. Aerosols in nature. Arch. Intern.Med. 131: 24-32, 1973.
2. HIDY, G.M. The dynamics of aerosols in the lower troposphere. In: Assessment of Airborne Particles. Edited by T.T. Mercer, P.E. Morrow, and W. Stober. Charles C Thomas: Springfield, Ill., 1971. pp.81-115
3. DEAN, G. Lung cancer among white South Africans. Br. Med. J. 2: 852-857, 1959.
4. AIR CONSERVATION COMMISSION AAAS. REPORT OF THE AAAS AIR CONSERVATION COMMISSION. WASHINGTON DC:American Association for the Advancement of Science, 1965.
5. TOP, F.H. Communicable and Infectious Diseases. C.V. Mosby Co.: St. Louis, 1964.
6. LIPPMAN, M., ALBERT, R.E., PETERSON, H.T. The regional deposition of inhaled aerosols in man. In: Inhaled Particles III. Edited by W.H. Walton.
7. FOORD, N., BLACK, A., WALSH, M. Pulmonary deposition of inhaled particles with diameters in the range 2.5 to 7.5 μ . In: Inhaled Particles IV. Edited by W.H. Walton. Pergamon press: New York, 1977, pp. 137-149.
8. FOORD, N., BLACK, A., WALSH, M. Regional deposition of 2.5-7.5 μ diameter inhaled particles in healthy male non-smokers. J. Aerosol Sci. 9: 343-357, 1978.
9. SCHLESINGER, R.B., LIPPMANN, M. Selective particle deposition and bronchogenic carcinoma. Environ. Res. 15: 424-431, 1978.
10. PAVIA, D., THOMSON, M., SHANNON, H.S. Aerosol inhalation and depth of deposition in the human lung. Arch. Environ. Health 32: 131-137, 1977.
11. STOKINGER, H.E., STEADMAN, L.T., WILSON, H.B., SYLVESTER, G.E., DZIUBA, S., LABELLE, C.W. Lobar deposition and retention of inhaled insoluble particles. Ind. Hyg. Occup. Med. 39: 346-353, 1951.

12. THOMAS, R.L., RAABE, O.G. Regional deposition of inhaled¹³⁷Cs-labeled monodisperse and polydisperse aluminosilicate aerosols in Syrian hamsters. Am. Ind. Hyg. Assoc. J. 39: 1009-1018, 1978.
13. BRAIN, J.D., KNUDSON, D.E., SOROKIN, S.P., DAVIS, M.A. Pulmonary distribution of particles given by intracheal instillation or by aerosol inhalation. Environ. Res. 11: 13-33, 1976.
14. PAVIA, D., THOMSON, M.L. The fractional deposition of inhaled 2 and 5 μ particles in the alveolar and tracheobronchial regions of the healthy human lung. Ann. Occup. Hyg. 19: 109-114, 1976.
15. ALBERT, R.E., LIPPMANN, M., PETERSON, H.T., BERGER, J., SANBORN, F., BOHNINE, D. Bronchial deposition and clearance of aerosols. Arch. Inter. Med. 131: 115-127, 1973.
16. TASK GROUP ON LUNG DYNAMICS. Deposition and retention models for internal dosimetry of the human respiratory tract. Health Phys. 12: 173-207, 1966.
17. LIPPMANN, M., ALBERT, R.E. The effect of particle size on the regional deposition of inhaled aerosols in the human respiratory tract. Am. Ind. Hyg. Assoc. J. 30: 257-275, 1969.
18. STEWART, B.O. Deposition of inhaled aerosols. Arch. Intern. Med. 131: 60-73, 1973.
19. THOMSON, M.L., PAVIA, D. Particle penetration and clearance in the human lung. Arch. Environ. Health 29: 214-219, 1974.
20. SANCHIS, J., DOLOVICH, M., CHAMBERS, R., NEWHOUSE, M.T. Regional distribution and lung clearance mechanisms in smokers and non-smokers. In: Inhaled Particles III. Edited by W.H. Walton. Unwin Brothers Limited, Gersham, Surrey, England, 1971. pp. 183-191.
21. EMMETT, P.C., AITKEN, R.J., MUIR, D.C.F. A new apparatus for use in studies of the total and regional deposition of aerosol particles in the human respiratory tract during steady breathing. J. Aerosol Sci. 10: 123-131, 1979.

22. DENNIS, W.L. The effect of breathing rate on the deposition of particles in the human respiratory system. In: Inhaled Particles III. Edited by W.H. Walton. Unwin Brothers Limited, Gresham Press, Surrey, England, 1971. pp. 91-105.
23. SCHLESINGER, R.B., LIPPMANN, M. Particle deposition in casts of the human upper tracheobronchial tree. Am. Ind. Hyg. Assoc. J. 33: 237-251, 1972.
24. SHAW, D.T., RAJENDRAN, N., LIAO, N.S. Theoretical modeling of fine-particle deposition in 3-dimensional bronchial bifurcations. Am. Ind. Hyg. Assoc. J. 39: 195-201, 197, 1978.
25. FUCHS, N.A., SUTUGIN, A.G. Generation and use of monodispersed aerosols. In: Aerosol Science. Edited by C.N. Davis. Academic press, New York, N.Y., 1966.
26. LOEB, L.B. The basic mechanisms of static electrification. Science 102: 573-576, 1945.
27. KUNKEL, W.B. The static electrification of dust particles on dispersion into a cloud. J. Appl. Phys. 21: 820-832.
28. SMOLUCHOWSKI, M. Experimentally demonstrable molecular phenomena which contradicts conventional thermodynamics. Phys. Z. 13: 1069-1080, 1912.
29. NATANSON, G.L. The electrification of drops during atomization of liquids as a result of fluctuations in the ion distribution. Zh Fiz Khim 23: 3034-314, 1949.
30. MERCER, T.T. Aerosol technology in hazard evaluation. Academic Press, New York, p. 7, 1964.
31. MERCER, T.T. Aerosol production and characterization: Some consideration for improving correlation of field and laboratory derived data. Health Physics 10: 873-887, 1964.
32. WHITBY, K.T. Homogenous Aerosol Generators. Tech. Rep. No. 13, Univ. of Minnesota, NP-10020, 1961.
33. SINCLAIR, D., LAMER, V.K. Light scattering as a measure of particle size in aerosols. Chem. Rev. 44: 245-267, 1949.

34. WILSON, I.B., LAMER, V.K. The retention of aerosol particles in the human respiratory tract: Experimental procedures and total deposition. Arch. Indust. Health 15: 293-303, 1957.
35. WALTON, W.H., PREWETT, W.C. The production of sprays and mists of uniform drop size by means of spinning disk. Proc. Phys. Soc. B62: 341-350, 1957
36. MAY, K.R. An improved spinning top homogeneous spray apparatus. J. Appl. Phys. 20: 932-938, 1949.
37. MAY, K.R. Spinning top homogeneous aerosol generator with shockproof mounting. J. Sci. Inst. 43: 841-842, 1966.
38. WHITBY, K.T., LUNDGEN, D.A., PETERSON, C.M. Homogenous aerosol generators. Int. J. Air Water Pollut. 9: 263-277, 1965.
39. LIPPMANN, M., ALBERT, R.E. A compact electric-motor driven spinning disk aerosol generator. Am. Ind. Hyg. Assoc. J. 28: 501-506, 1967.
40. RABBE, O. The dilution of monodispersed suspensions for aerosolization. Am. Ind. Hyg. Assoc. J. 29: 439-443, 1968.
41. RABBE, O. The generation of aerosols of fine particles. In: Fine Particles. Edited by B.Y.H. Liu. Academic Press, New York, 1971.
42. BISA, K., DIRNAGL, K., ESCHE, R. Zerstaubung von flussigkeiten mit ultraschall. Seimens Z 28: 341-347, 1954.
43. LANG, R.J. Ultrasonic atomization of liquids. J. Acoust. Soc. Am. 34: 6-8, 1962.
44. BOGUSLAVSKI, Y.Y., EKNADIOSYANTS, O.K. Physical mechanisms of the acoustic atomization of a liquid. Akust. Zh. 15: 14-21, 1969.
45. MERCER, T.T. Production and characterization of aerosols. Arch. Intern. Med. 131: 39-50, 1973.
46. MERCER, T.T., GODDARD, R.F., FLORES, R.L. Output characteristics of several commercial nebulizers. Ann. Allergy 23: 314-326, 1965.
47. MERCER, T.T., GODDARD, R.F., FLORES, R.L. Output characteristics of three ultrasonic nebulizers. Ann. Allergy 26: 18-27, 1968.

48. MERCER, T.T., TILLERY, M.I., CHOW, H.Y. Operating characteristics of some compressed-air nebulizers. *Am. Ind. Hyg. Assoc. J.* 29: 66-78, 1968.
49. LARSON, E.W., YOUNG, H.W., WALKER, J.S. Aerosol evaluations of the DeVilbiss No. 40 and Vaponefrin nebulizers. *Appl. Environ. Micro.* 31: 150-151, 1976.
50. REIF, A.E., HOLCOMB, M.P. Operating characteristics of commercial nebulizers and their adaptation to produce closely sized aerosols. *Ann. Allergy* 16: 626-638, 1958.
51. DAVIES, C.N., AYLWARD, NM., LEACEY, D. Impingement of dust from airjets. *A.M.A. Arch. Ind. Health Occ. Med.* 4: 354-397, 1951.
52. MAY, K.R. The Cascade Impactor: An instrument for sampling coarse aerosols. *J. Sci. Inst.* 22: 187-195, 1945.
53. SWIFT, D.L. Aerosols and humidity therapy: Generation and respiratory deposition of therapeutic aerosols. *Am. Rev. Respir. Dis.* 122: 71-77, 1980.
54. REIF, A.E., MITCHELL, C. Size analysis of water aerosols. *Ann. Allergy* 17: 157-172, 1959.
55. PORSTENDORFER, J., GEBHART, J., ROBIG, G. Effect of evaporation on the size distribution of nebulized aerosols. *J. Aerosol Sci.* 8: 371-380, 1977.
56. DAUTREBANDE, L., WALKENHORST, W. In: Inhaled Particles and Vapours. Edited by C.N. Davies. Pergamon Press, Oxford. 1971.
57. FERRON, G.A. The size of soluble aerosol particles as a function of the humidity of the air. Application to the human respiratory tract. *J. Aerosol Sci.* 8: 251-267, 1977.
58. LANDAHL, H.D., TRACEWELL, T.N., LASSEN, W.H. On the retention of airborne particles in the human lung. *Arch. Ind. Hyg. Occ. Med.* 3: 356-366, 1951.
59. BRAIN, J.D., VALBERG, P.A. Deposition of aerosol in the respiratory tract. *Am. Rev. Respir. Dis.* 120: 1325-1373, 1979.

60. LANDAHL, H.D. On the removal of airborne droplets by the human respiratory tract. I. The Lung. Bull. Math. Biophys. 12: 161-169, 1950.
61. HATCH, T., GROSS, P. Pulmonary Deposition and Retention of Inhaled Aerosols Academic Press, New York, 1964.
62. WEIBEL, E.R. Morphometry of the Human Lung Springer-Verlag, Berlin, 1963.
63. HAYEK, H.V. The Human Lung Hafner, New York, 1960.
64. HATCH, T., HEMON, W.L.C. Influence of particle size in dust exposure. J. Ind. Hyg. Toxicol. 30: 172-180, 1948.
65. WILSON, I.B., LAMER, V.K. The retention of aerosol particles in the human respiratory tract as a function of particle radius. J. Ind. Hyg. Toxicol. 30: 265-280, 1948.
66. GESSNER, H., RUTTNER, J.R., BUHLER, H. Zur bestimmung des korngrossenbereiches von silikogenem staub. Schweiz Med. Wochenschr. 79: 1258-1262, 1949.
67. BROWN, J.H., ET AL. Influence of particle size upon the retention of particulate matter in the human lung. Am. J. Public Health 40: 450-458, 1950.
68. BEECKMANS, J.M. The deposition of aerosols in the respiratory tract. (1) Mathematical analysis and comparison with experimental data. Can. J. Physiol. Pharmacol. 43: 157-172, 1965.
69. STAHLHOFEN, W., GEBHART, J., HEYDER, J. Experimental determination of the regional deposition of aerosol particles in the human respiratory tract. Am. Ind. Hyg. Assoc. J. 41: 385-398a, 1980.
70. YU, C.P., TAULBEE, D.B. A theory of predicting respiratory tract deposition of inhaled particles in man. In: Inhaled Particles IV. Edited by W.H. Walton. Pergamon Press, New York, 1977. pp. 35-47.
71. DAVIES, C.N. Deposition of inhaled particles in man. Chemistry in Industry 1974. pp. 441-444.

72. HEYDER, J., GEBHART, J., ROTH, C., STAHLHOFEN, W., STUCK, B., TARRONI, G., DEZAIACOMO, T., FORMIGNANI, M., MELANRI, C., PRODI, V. Intercomparison of lung deposition data for aerosol particles. *J. Aerosol Sci.* 9: 147-155, 1978.
73. DAVIES, C.N., LEVER, M.J., ROTHENBERG, S.J. Experimental studies of the deposition of particles in the human lung. In: Inhaled Particles IV. Edited by W.H. Walton. Pergamon Press, New York, 1977. pp.151-162.
74. THOMSON, M.L., PAVIA, D. Particle penetration and clearance in the human lung. *Arch. Environ. Health* 29: 214-219, 1974.
75. THOMSON, M.L., SHORT, M.D. Mucociliary function in health, chronic obstructive airway disease, and asbestosis. *J. Appl. Physiol.* 26: 535-539, 1969.
76. LIPPMAN, M., ALBERT, R.E., PETERSON, H.T. The regional deposition of inhaled aerosols in man. In: Inhaled Particles III. Edited by W.H. Walton. Unwin Brothers Limited, Gresham press, 1971. pp. 105-122.
77. TAPLIN, G.V., CHOPRA, S.K. Lung Perfusion-Inhalation: Scintigraphy in obstructive airway disease and pulmonary embolism. *Radiol. Clin. North Am.* XVI: 491-513, 1978.
78. TAPLIN, G.V. ET AL. Early detection of chronic obstructive pulmonary disease using radionuclide lung-imaging procedures. *Chest* 71: 567-575, 1977.
79. LIPPMAN, M., ALBERT, R.E., YEATES, D.B., BERGER, J.M., FOSTER, W.M., BOHNING, D.E. Factors affecting tracheobronchial mucociliary transport. In: Inhaled Particles IV. Edited by W.H. Walton. Pergamon Press, New York, 1977. pp. 305-319.
80. MATSUBA, K., THURLBECK, W.M. The number and dimensions of small airways in nonemphysematous lungs. *Am. Rev. Respir. Dis.* 104: 516-524. 1971.
81. SCHLESINGER, R.B., LIPPMANN, M. Selective particle deposition and bronchogenic carcinoma. *Environ. Res.* 15: 424-431, 1978.

82. LARSON, S.A. Gamma Camera Emission Tomography,
Supplementum 363, Acta Radiologica Typografia,
Goteborg, Sweden, 1980.
83. SOUSSALINE, F.P., TODD-POLROPEK, A.E., ZUROWSKI, S.,
HUFFER, E., RAYNAUD, C.E. KELLERSHOHN, C.L. A
rotating conventional gamma camera single-photon
tomographic system: Physical characterization.
J. Comput. Assist. Tomogr. 5: 551-556, 1981.
84. EARLY, P.J., RAZZAK, M.A., SODEE, D.M. Textbook of
Nuclear Medicine Technology. 2 nd Edition
C.V.Mosby Co.:St. Louis, 1975
85. SCOTT, J. Personal communication.
86. MUIR, D.C.F., DAVIES, C.N. Ann. Occup. Hyg. 10:
161-174, 1967 Cited by Davies, C.N., Lever, M.J.
Rothenberg, S.J. Experimental studies of the
deposition of particles in the human respiratory
lung. In: Inhaled Particles IV. Edited by W.H.
Walton. Pergamon Press, New York, 1977. p. 151.
87. SNYDER, W.J., FORD, M.R., WARNER, G.G., WATSON, S.B.
Medical internal radiation dose, pamphlet #11,
Oak Ridge National lab, Oak Ridge, Tennessee.
88. ROEDLER, H.D., KAUL, A., HINE, G.J. Internal
Radiation Dose in Diagnostic Nuclear Medicine.
Verlag H. Hoffmann Berlin, 1978.
89. DENNIS, R. (Ed) HANDBOOK ON AEROSOLS Published by
the Technical Information Center Energy Research
& Development Administration, 1976.

GENERAL BIBLIOGRAPHY

- ALBERT, R.E., LIPPMANN, M., PETERSON, H.T., BERGER, J., SANBORN, F., BOHNINE, D. Bronchial deposition and clearance of aerosols. *Arch. Inter. Med.* 131: 115-127, 1973.
- ANDERSEN, I., CAMNER, P., JENSEN, P.L. A comparison of nasal and tracheobronchial clearance. *Arch. Environ. Health* 29: 290-293, 1974.
- ASMUDSSON, T., JOHNSON, R.F., KILBURN, K.H., GOODRICH, J.K. Efficiency of nebulizers for depositing saline in human lung. *Am. Rev. Respir. Dis.* 108: 506-512, 1973.
- AURNHAMMER, W., KONIETZKO, N., MATTHYS, H. Problems in evaluating the effect of secretolytic agents on the mucociliary system by means of radioactive particles. *Respiration* 34: 92-99, 1977.
- BAKER, H., GRIFFITHS, J.C. The size of water droplets in relation to the treatment of the obstructive respiratory ills of childhood. *Am. Rev. Respir. Dis.* 97: 1131-1140, 1968.
- BATEMAN, J.R., NEWMAN, S.O., DAUNT, K.M., PAVIA, D., CLARKE, S.W. Regional lung clearance of excessive bronchial secretions during chest physiotherapy in patients with stable chronic airways obstruction. *Lancet* 1: 294-297, 1979.
- BATES, D.V. Measurement of regional ventilation and blood flow distribution. *Handbook Physiol. Respir.* II: 1425-1436, 1965.
- BAU, S.K., ASPIN, N., WOOD, D.E., LEVISON, H. The measurement of fluid deposition in humans following mist tent therapy. *Pediatrics* 48: 605-612, 1971.
- BELL, K.A., FRIEDLANDERS, S.K. Aerosol deposition in models of a human lung bifurcation. *Staub Reinhaltung der Luft (in English)* 33: 183-187, 1973.
- BERGMAN, L.V., SILSON, J.E. Particle size produced by various instruments for inhalation therapy. *Ann. Allergy* 19: 735-748, 1961.
- BRAIN, J.D., KNUDSON, D.E., SOROKIN, S.P., DAVIS, M.A. Pulmonary distribution of particles given by intracheal instillation or by aerosol inhalation. *Environ. Res.* 11: 13-33, 1976.

- BRIAN, J. Aerosol and humidity therapy. Am. Rev. Respir. Dis. 122:(Part II), 1980.
- BRIAN, J.D., VALBERG, P.A. Deposition of aerosol in the respiratory tract. Am. Rev. Respir. Dis. 120: 1325-1373, 1979.
- CHEN, W.J.R., SHIAH, D.S.P., WANG, C.S. A three-dimensional model of the upper tracheobronchial tree. Bull. Math. Biol. 42: 847-859, 1980.
- CHERVU, L.R., VALLABHAJOSULA, S.R., BLAUFox, M.D. Quality control of technetium labelled lung imaging agents. Int. J. Nucl. Med. Biol. 4: 201-203, 1977.
- CHOPRA, S.K., TAPLIN, G.V., TASHKIN, D.P., ELAM, D. Lung clearance of soluble radioaerosols of different molecular weights in systemic sclerosis. Thorax 34: 63-67, 1979.
- DAVIES, C.N., LEVER, M.J., ROTHENBERG, S.J. Experimental studies of the deposition of particles in the human lung. In: Inhaled Particles IV. Edited by W.H. Walton. Pergamon Press, New York, 1977. pp. 151-162.
- DENNIS, W.L. The effect of breathing rate on the deposition of particles in the human respiratory system. In: Inhaled Particles III. Edited by W.H. Walton. Unwin Brothers Limited, Gresham Press, Surrey, England, 1971. pp. 91-105.
- EMMETT, P.C., AITKEN, R.J., MUIR, D.C.F. A new apparatus for use in studies of the total and regional deposition of aerosol particles in the human respiratory tract during steady breathing. J. Aerosol Sci. 10: 123-131, 1979.
- ETTINGER, H.J., POSNER, S. Evaluation of particle sizing and aerosol sampling techniques. Am. Ind. Hyg. Assoc. J. 25: 17-25, 1965.
- FERRON, G.A. The size of soluble aerosol particles as a function of the humidity of the air. Application to the human respiratory tract. J. Aerosol Sci. 8: 251-267, 1977.
- FEW, J.D., SHORT, M.D., THOMSON, M.L. Preparation of ^{99m}Tc labelled particles for aerosol studies. Radiochem. Radioanal. Letters 5: 275-277, 1970.

- FOORD, N., BLACK, A., WALSH, M. Regional deposition of 2.5-7.5 μ diameter inhaled particles in healthy male non-smokers. *J. Aerosol Sci.* 9: 343-357, 1978.
- FOORD, N., BLACK, A., WALSH, M. Pulmonary deposition of inhaled particles with diameters in the range 2.5 to 7.5 μ . In: *Inhaled Particles IV*. Edited by W.H. Walton. Pergamon Press: New York, 1977. pp. 137-149.
- FOSTER, W.M., LANGENBACK, E., BERGOFKY, E.H. Measurement of tracheal and bronchial mucus velocities in man: Relation to lung clearance. *Am. Physiol. Soc.* : 965-971, 1980.
- GREEN, G.M., JAKAB, G.J., LOW, R.B., DAVIS, G.S. Defence mechanisms of the respiratory membrane. *Am. Rev. Respir. Dis.* 115: 479-513, 1977.
- GROSSMAN, Z.D., GAGNE, G., ZENS, A., THOMAS, F.D., CHAMBERLAN, C.C., SINGH, A., COHEN, W., HEITZMAN, E.R. Transmission computed tomography; Tc-99m MAA scintigraphy, and plain chest radiography after experimentally produced acute pulmonary arterial occlusion in the dog. *J. Nucl. Med.* 20: 1251-1256, 1979.
- GUR, D., DRAYER, B.P., BOROVETZ, H.S., GRIFFITH, B.P., HARDESTY, R.L. WOLFSON, S.K. Dynamic computed tomography of the lung: Regional ventilation measurements. *J. Comput. Assist. Tomogr.* 3: 749-753, 1979.
- HAYES, M., TAPLIN, G.V., CHOPRA, S.K., KNOX, D.E., ELAM, D. Improved radioaerosol administration system for routine inhalation lung imaging. *Radiology* 131: 256-258, 1979.
- HEYDER, J., GEBHART, J., STAHLHOFEN, W. Inhalation of aerosols: Particle deposition and retention. In: *Generation of Aerosols*. Edited by Klaus Willeke. Ann Arbor Science Publishers, Ann Arbor, MI, 1980. pp. 65-103.
- HEYDER, J., GEBHART, J., ROTH, C., STAHLHOFEN, W., STUCK, B., TARRONI, G., DEZAIACOMO, T., FORMIGNANI, M., MELANRI, C., PRODI, V. Intercomparison of lung deposition data for aerosol particles. *J. Aerosol Sci.* 9: 147-155, 1978.
- HISATOSHI, M., ITOH, H., IJHII, Y., MAKAI, J., TODD, G., FUJITA, J., TORIZUKA, K. Determination of the pleural edge by gamma-ray transmission computed tomography. *J. Nucl. Med.* 22: 815-817, 1981.

- HOGG, J.C., MACKLEM, P.T., THURLBECK, W.M. Site and nature of airway obstruction in chronic obstructive lung disease. *N. Engl. J. Med.* 278: 1355-1360, 1968.
- HUGES, J.M.B., GLAZIER, J.B., MALONEY, J.E. Effect of lung volume on the distribution of pulmonary blood flow in man. *Respir. Physiol.* 4: 58-72, 1968.
- JASZCAK, R.J., CHANG, L.T., STEIN, N.A., MOORE, F.E. Whole body single photon emission computed tomography using dual, large-field-of-view scintillation cameras. *Phys. Med. Biol.* 24: 1123-1143, 1979.
- JONES, J.G., MINTY, B.D., LAWLER, P., HURANS, G., CRAWLEY, J.C.W., VEALL, N. Increased alveolar epithelial permeability in cigarette smokers. *Lancet* 1: 66-68, 1980.
- KHAN, O., ELL, P.J., JARRITT, P.H., CULLUM, I., WILLIAMS, E.S. Radionuclide section scanning of the lungs in pulmonary embolism. *Br. J. Radiol.* 54: 586-591, 1981.
- KONIETZKO, N., MULLER, M., MATTHY, S.H. Quantitative and selective bronchial clearance studies using ^{99m}Tc -sulfate particles. *Scand. J. Respir. Dis.* 85: 33-37, 1974.
- KOTRAPPA, P., RAGHONATH, B., SUBRAMONAYAN, RAIKAR, U.R., SHARMA, S.M. Scintiphotography of lungs with dry aerosol generation and delivery system: Concise communication. *J. Nucl. Med.* 18: 1082-1085, 1977.
- LAPPLE, C.E. Particle size analysis and analyzers. *Chem. Engineering* 75: 149-156, 1968.
- LARSON, E.W., YOUNG, H.W., WALKER, J.S. Aerosol evaluations of the DeVilbiss No. 40 and Vaponefrin nebulizers. *Appl. Envir. Micro.* 31: 150-151, 1976.
- LIN, M.S., GOODWIN, D.A. Pulmonary distribution of an inhaled radioaerosol in obstructive pulmonary disease. *Radiology* 118: 645-651, 1976.
- LIN, M.S., HAYES, T.M., GOODWIN, D.A., KRUSE, S.L. Distal penetration in radioaerosol inhalation with an ultrasonic nebulizer. *Radiology* 112: 443-447, 1974.
- LIPPMAN, M., ALBERT, R.E. The effect of particle size on the regional deposition of inhaled aerosols in the human respiratory tract. *Am. Ind. Hyg. Assoc. J.* 30: 257-275, 1969.

- LIPPMAN, M., ALBERT, R.E., PETERSON, H.T. The regional deposition of inhaled aerosols in man. In: Inhaled Particles III. Edited by W.H. Walton. Unwin Brothers Limited, Gresham Press, 1971. pp. 105-122.
- LIPPMAN, M., ALBERT, R.E., YEATES, D.B., BERGER, J.M., FOSTER, W.M., BOHNING, D.E. Factors affecting tracheobronchial mucociliary transport. In: Inhaled Particles IV. Edited by W.H. Walton. Pergamon Press: New York, 1977. pp. 305-319.
- LOURENCO, R.V., KLIMEK, M.F., BOROWSKI, C.J. Deposition and clearance of 2 μ particles in the tracheobronchial tree of normal subjects - smokers and nonsmokers. J. Clin. Invest. 50: 1411-1420, 1971.
- LOVE, R.G., MUIR, C.F., SWEETLAND, K.F. Aerosol deposition in the lungs of coalworkers. In: Inhaled Particles III. Edited by W.H. Walton. Unwin Brothers Limited, Gresham press, 1971. pp. 131-139.
- LUCHSINGER, P.C., LAGARDE, B., KILFEATHER, J.E. Particle clearance from the human tracheobronchial tree. Am. Rev. Respir. Dis. 97: 1046-1050, 1968.
- MARPLE, V.A. Stimulation of respirable penetration characteristics by inertial impaction. J. Aerosol Sci. 9: 125-134, 1978.
- MAY, K.R. The collison nebulizer: Description, performance and application. Aerosol Sci. 4: 235-243, 1973.
- MAY, K.R. An improved spinning top homogeneous spray apparatus. J. Appl. Phys. 20: 932-938, 1949.
- MAY, K.R. Spinning top homogeneous aerosol generator with shockproof mounting. J. Sci. Inst. 43: 841-842, 1966.
- MERCER, T.T. Production and characterization of aerosols. Arch. Intern. Med. 131: 39-50, 1973.
- MERCER, T.T., GODDARD, R.F., FLORES, R.L. Output characteristics of several commercial nebulizers. Ann. Allergy 23: 314-326, 1965.
- MERCER, T.T., GODDARD, R.F., FLORES, R.L. Output characteristics of three ultrasonic nebulizers. Ann. Allergy 26: 18-27, 1968.

- MERCER, T.T., TILLERY, M.I., CHOW, H.Y. Operating characteristics of some compressed-air nebulizers. *Am. Ind. Hyg. Assoc. J.* 29: 66-78, 1968.
- MITHOEFER, J.C. Mechanism of pulmonary gas exchange and CO₂ transport during breath holding. *J. Appl. Physiol.* 14: 706-710, 1959.
- MITHOEFER, J.C. Lung volume restriction as a ventilatory stimulus during breath holding. *J. Appl. Physiol.* 14: 701-705, 1959.
- MORROW, P.E., GIBB, F.R., GAZIOFLU, K.M. A study of particulate clearance from the human lungs. *Am. Rev. Respir. Dis.* 96: 1209-1221, 1967.
- NEWHOUSE, M., SANCHIS, J., BIENENSTOCK, J. Lung defence mechanisms Part I. *N. Engl. J. Med.* 295: 990-998, 1976.
- NEWHOUSE, M., SANCHIS, J., BIENENSTOCK, J. Lung defence mechanisms Part II. *N. Engl. J. Med.* 295: 1045-1052, 1976.
- NEWTON, G.J., RAABE, O.G., MOKLER, B.V. Cascade impactor design and performance. *J. Aerosol Sci.* 8: 334-347, 1977.
- ORR, C. JR., HURD, F.K., CORBETT, W.J. Aerosol size and relative humidity. *J. Colloid Sci.* 13: 472-482, 1958.
- PALMES, E.D., LIPPMANN, M. Influence of respiratory air space dimensions on aerosol deposition. In: *Inhaled Particles IV*. Edited by W.H. Walton. Pergamon Press, New York, 1977. pp. 127-136.
- PAVIA, D., THOMSON, M., SHANNON, H.S. Aerosol inhalation and depth of deposition in the human lung. *Arch. Environ. Health* 32: 131-137, 1977.
- PAVIA, D., THOMSON, M.L. The fractional deposition of inhaled 2 and 5 μ particles in the alveolar and tracheobronchial regions of the healthy human lung. *Ann. Occup. Hyg.* 19: 109-114, 1976.
- PIRCHER, F.J., KNIGHT, C.M., BARRY, W.F., TEMPLE, J.R., KIRSCH, W.J. Retention, distribution and absorption of inhaled albumin aerosol and absorbed dose estimates from its' I¹³¹ and Tc^{99m} labels. *Am. J. Roentgenol.* 100: 813-821, 1967.

- POE, N.D., COHEN, M.B., YANDA, R.L. Application of delayed lung imaging following radioaerosol inhalation. *Radiology* 122: 739-746, 1977.
- PORSTENDORFER, J., GEBHART, J., ROBIG, G. Effect of evaporation on the size distribution of nebulized aerosols. *J. Aerosol Sci.* 8: 371-380, 1977.
- PROCTOR, D.F. The upper airways. *Am. Rev. Respir. Dis.* 115: 97-129, 1977.
- RAIKAR, U.R., GANATRA, R.D., RAGHUNATH, G. Dry aerosol delivery system compared to ultrasonic nebulizer. *J. Nucl. Med.* 19: 1088, 1978.
- RAO, A.K., WHITBY, K.T. Non-ideal collection characteristics of inertial impactors. I. Single-stage impactors and solid particles. *J. Aerosol Sci.* 9: 77-86, 1978.
- RAO, A.K., WHITBY, K.T. Non-ideal collection characteristics of inertial impactors. II. Cascade impactors. *J. Aerosol Sci.* 9: 87-100, 1978.
- REIF, A.E., HOLCOMB, M.P. Operating characteristics of commercial nebulizers and their adaptation to produce closely sized aerosols. *Ann. Allergy* 16: 626-638, 1958.
- REIF, A.E., MITCHELL, C. Size analysis of water aerosols. *Ann. Allergy* 17: 157-172, 1959.
- RINDERKNECHT, J., SHAPIRO, L., KRAYTHAMMER, M., TAPLIN, G., WASSERMAN, K., USZLER, J.M., EFFROS, R.M. Accelerated clearance of small solutes from the lungs in interstitial lung disease. *Am. Rev. Respir. Dis.* 121: 105-117, 1980.
- ROBINSON, A.E., GOODRICH, J.K., SPOCK, A. Inhalation and perfusion radionuclide studies of pediatric chest disease. *Radiology* 93: 1127-1128, 1969.
- ROSS, I.T.H., WALLACE, J.C., WAITE, D. A simplified method of monitoring mucociliary transport. *Br. J. Radiol.* 52: 968-971, 1979.
- RUHLE, K.H., KOHLER, D., FISCHER, J., MATTHYS, H. Measurements of mucociliary clearance with ^{99m}Tc -tagged erythrocytes. *Prog. Resp. Res.* 11: 117-126, 1979.

- SANCHIS, J., DOLOVICH, M., CHALMERS, R., NEWHOUSE, M.
Quantitation of regional aerosol clearance in the
normal human lung. *J. Appl. Physiol.* 33: 757-
762, 1972.
- SANCHIS, J., DOLOVICH, M., CHAMBERS, R., NEWHOUSE, M.T.
Regional distribution and lung clearance mechanisms
in smokers and non-smokers. In: Inhaled Particles
III. Edited by W.H. Walton. Unwin Brothers
Limited, Gersham, Surrey, England, 1971. pp.
183-191.
- SCHLESINGER, R.B., LIPPMANN, M. Selective particle
deposition and bronchogenic carcinoma. *Environ.
Res.* 15: 424-431, 1978.
- SCHLESINGER, R.B., LIPPMANN, M. Particle deposition in
casts of the human upper tracheobronchial tree.
Am. Ind. Hyg. Assoc. J. 33: 237-251, 1972.
- SHAW, D.T., RAJENDRAN, N., LIAO, N.S. Theoretical modeling
of fine-particle deposition in 3-dimensional
bronchial bifurcations. *Am. Ind. Hyg. Assoc. J.*
39: 195-201, 1978.
- SOLER, M., ROBERT, M., ANFOSSO, F., BOUFFANT, L. Technical
procedure for tagged pollen aerosols for the study
of their penetration in the bronchial tree. *Bull.
Physiopathol. Respir.* 13: 499-511, 1977.
- SOUSSALINE, F.P., TODD-POLROPEK, A.E., ZUROWSKI, S., HUFFER,
E., RAYNAUD, C.E., KELLERSHOHN, C.L. A rotating
conventional gamma camera single-photon tomographic
system: Physical characterization. *J. Comput.
Assist. Tomogr.* 5: 551-556, 1981.
- SPRITZER, A.A., WATSON, J.A., AULD, J.A. Clearance rates
determinants: Parameters influencing clearance
rates of particles in the upper respiratory
tract. In: Inhaled Particles III. Edited by W.H.
Walton. Unwin Brothers Limited, Gresham Press,
Surrey, England, 1971. pp. 149-182.
- STAHLHOFEN, W., GEBHART, J., HEYDER, J., PHILIPSON, K.,
CAMNER, P. Intercomparison of regional deposition
of aerosol particles in the human respiratory tract
and their long-term elimination. *Exp. Lung Res.*
2 131-139, 1980.
- STAHLHOFEN, W., GEBHART, J., HEYDER, J. Experimental
determination of the regional deposition of
aerosol particles in the human respiratory tract.
Am. Ind. Hyg. Assoc. J. 41: 385-398a, 1980.

- STERN, E.L., JOHNSON, J.W., VESLEY, D., HALBERT, M.M., WILLIAMS, L.E. Aerosol production associated with clinical laboratory procedures. *Am. J. Clin. Pathol.* 62: 591-600, 1974.
- STEWART, B.O. Deposition of inhaled aerosols. *Arch. Intern. Med.* 131: 60-73, 1973.
- STOKINGER, H.E., STEADMAN, L.T., WILSON, H.B., SYLVESTER, G.E., DZIUBA, S., LABELLE, C.W. Lobar deposition and retention of inhaled insoluble particles. *Ind. Hyg. Occup. Med.* 39: 346-353, 1951.
- SWIFT, D.L. Aerosols and humidity therapy: Generation and respiratory deposition of therapeutic aerosols. *Am. Rev. Respir. Dis.* 122: 71-77, 1980.
- TAPLIN, G., CHOPRA, S.K., USZLER, J.M. Imaging experimental pulmonary ischemic lesions after inhalation of a diffusible radioaerosol - recent and further developments. *J. Nucl. Med.* 19: 567-568, 1978.
- TAPLIN, G.V., POE, N.D. A dual lung-scanning technique for evaluation of pulmonary function. *Radiology* 85: 365-368, 1965.
- TAPLIN, G.V. The history of lung imaging with radionuclides. *Semin. Nucl. Med.* IX: 178-185, 1979.
- TAPLIN, G.V., CHOPRA, S.K. Lung Perfusion-Inhalation: Scintigraphy in obstructive airway disease and pulmonary embolism. *Radiol. Clin. North Am.* XVI: 491-513, 1978.
- TAPLIN, G.V., CHOPRA, S.K. Inhalation lung imaging with radioactive aerosols and gases. *Prog. Nucl. Med.* 5: 119-143, 1970.
- TAPLIN, G.V., CHOPRA, S.K., ELAM, D. Imaging experimental pulmonary ischemic lesions after inhalation of a defusible radioaerosol: Concise communication. *J. Nucl. Med.* 18: 250-254, 1977.
- TAPLIN, G.V., HAYES, M. Lung imaging with radioactive aerosols for the assessment of airway disease. *Semin. Nucl. Med.* 10: 243-251, 1980.
- TASK GROUP ON LUNG DYNAMICS. Deposition and retention models for internal dosimetry of the human respiratory tract. *Health Phys.* 12: 173-207, 1966.

- THOMAS, R.L., RAABE, O.G. Regional deposition of inhaled ^{137}Cs -labeled monodisperse and polydisperse aluminosilicate aerosols in Syrian hamsters. *Am. Ind. Hyg. Assoc. J.* 39: 1009-1018, 1978.
- THOMSON, M.L., PAVIA, D. Particle penetration and clearance in the human lung. *Arch. Environ. Health* 29: 214-219, 1974.
- THOMSON, M.L., SHORT, M.D. Mucociliary function in health, chronic obstructive airway disease, and asbestosis. *J. Appl. Physiol.* 26: 535-539, 1969.
- TILLERY, M.I., WOOD, G.D., ETTINGER, H.J. Generation and characterization of aerosols and vapors for inhalation experiments. *Environ. Health Perspect.* 16: 25-40, 1976.
- TOMENIUS, L. Deposition of 2 and 7 μ particles in the rabbit lung. *Am. Rev. Respir. Dis.* 115: 29-32, 1977.
- WALSH, M., BLACK, A., FOORD, N. Apparatus for the administration by inhalation of radioactive particles to human subjects for studies of deposition and clearance. *J. Aerosol Sci.* 8: 83-90, 1977.
- WANNER, A. Clinical aspects of mucociliary transport. *Am. Rev. Respir. Dis.* 116: 73-126, 1977.
- WARDICK, A., EGE, G.N., HENKELMAN, R.M., MAIER, G., LYSTER, D.M. An evaluation of radiocolloid sizing techniques. *J. Nucl. Med.* 18: 827-834, 1977.
- WASNICH, R.D. A high-frequency ultrasonic nebulizer system for radioaerosol delivery. *J. Nucl. Med.* 17: 707-710, 1976.
- WOLFF, R.K., DOLOVICH, M., OBMINSKI, G., NEWHOUSE, M.T. Effect of sulphur dioxide on tracheobronchial clearance at rest and during exercise. pp. 321-332.
- YEATES, D.B., ASPIN, N., BRYAN, A.C., LEVISON, H. Regional clearance of ions from the airways of the lung. *Am. Rev. Respir. Dis.* 107: 602-608, 1973.
- YEATES, D.B., ASPIN, N., LEVISON, H., JONES, M.T., BRYAN, A.C. Mucociliary tracheal transport rates in man. *J. Appl. Physiol.* 39: 487-495, 1975.

- YEATES, D.B., WARBICK, A., ASPIN, N. Production of ^{99m}Tc labelled albumin microspheres for lung clearance studies and inhalation scanning. *Int. J. Appl. Radiat. Isot.* 25: 578-580, 1974.
- YU, C.P., TAULBEE, D.B. A theory of predicting respiratory tract deposition of inhaled particles in man. In: Inhaled Particles IV. Edited by W.H. Walton. Pergamon Press, New York, 1977. pp. 35-47.

APPENDIX I TABLE XI

SUMMARY OF THE AEROSOL SIZING TRIALS CARRIED OUT WITH THE BENDIX ULTRASONIC NEBULIZER

RUN #	ULTRASONIC SETTING	IMPACTOR LENGTH (cm)	TUBING	COMPOUND	LABEL	AMAD (μm)	σg	COMMENTS
1.	Hi	15		sulphur colloid	99mTc	2.50	1.56	
2.	Hi	45		sulphur colloid	99mTc	2.13	1.47	
3.	80% of Max.	25		normal saline	none	2.60 (MMD)	1.93	Sized by gravimetric analysis.
4.	Hi	15		sulphur colloid	99mTc	4.1	1.8	A modified colloid prep. using 10 min. heating time vs normal $3\frac{1}{2}$ min.
5.	Hi	30		sulphur colloid and gelatin	99mTc	1.3 est.	NA	0.10 gm of gelatin added to 2.0 ml sulphur colloid to increased density of solution. Very low output activity noted.
6.	Hi	45		Sorin HSA microspheres	99mTc	3.15	1.47	Microspheres are reported to be less than 0.5 μm .
7.	Bi	NA		MAA	99mTc	2.70 (MMD)	2.23	Sized by gravimetric analysis.
8.	Hi	15		$^{152}\text{Sm}203$	153Sm	1.9	1.3	Labelled in the SLOWPOKE REACTOR.

APPENDIX 2 TABLE XII

SUMMARY OF THE AEROSOL SIZING TRIALS CARRIED OUT WITH AIRLIFE AND HUDSON NEBULIZERS

MAKE	MODEL	GENERATOR TO IMPACTOR TUBING LENGTH (cm)	COMPOUND	LABEL	PRESSURE (PSI)	AMAD (μm)	σ_g	COMMENTS
Hudson	1712	18	sulphur colloid	99 ^m Tc	20	1.74	1.75	Internal impinger, at 50% of normal height.
Hudson	1712	15	sulphur colloid	99 ^m Tc	20	1.4	3.2	Air jet drilled to 150% normal size. No impinger
Hudson	1712	15	sulphur colloid	99 ^m Tc	20	1.3	2.0	Drilled out as above. Internal impinger raised 50% above normal.
Airlife Misty- neb		20	sulphur colloid	99 ^m Tc	20	1.72	2.25	Gave a bimodal distribution of particle sizes.

APPENDIX 3 Table XIII

SUMMARY OF THE AEROSOL SIZING TRIALS CARRIED OUT WITH THE DEVILBISS NEBULIZER

RUN #	MODEL	COMPOUND	LABEL	PRESSURE (PSI)	BAG-IN-BOX	AMAD (µm)	σg	COMMENTS
1	45	sulphur colloid	99 ^m Tc	30	Yes	1.50	2.3	
2	45	sulphur colloid	99 ^m Tc	20	Yes	1.32	1.67	Vent out, 5-10 seconds settling time.
3	45	sulphur colloid	99 ^m Tc	20	Yes	1.45	1.71	Vent in, 15 seconds settling time.
4	45	Metha-choline (25mg/ml)	None	20	No	1.15 (MMD)	2.0	Impactor connected to nebulizer directly via 15cm of tubing. Gravimetric analysis.
5	40	normal saline	None	30	Bag only	1.1 (MMD)	1.85	Gravimetric analysis.
6	40	sulphur colloid	99 ^m Tc	30	Bag only	1.18	1.82	
7	40	sulphur colloid	99 ^m Tc	20	Yes	1.25	1.69	15 sec. settling time in bag.
8	40	sulphur colloid	99 ^m Tc	30	Yes	1.18	1.71	45 sec. settling time in bag.
9	40	sulphur colloid	99 ^m Tc	20	Yes	1.27	1.84	45 sec. settling time in bag.

TABLE XIII (cont'd)

RUN #	MODEL	COMPOUND	LABEL	PRESSURE ° (PSI)	BAG-IN-BOX	AMAD σg (μm)	COMMENTS
10	40	normal saline	Tc04	30	Yes	0.70 1.92	Newer model 40.
11	40	sulphur colloid	99mTc	30	Yes	0.93 1.74	Older model 40
12	40	sulphur colloid	99mTc	30	Yes	1.20 1.64	15 second settling time sample taken with inlet valve of Rudolf valve removed.
13	40	sulphur colloid	99mTc	30	No	0.96 1.73	30cm tubing between nebulizer and impactor.
14	40	sulphur colloid	99mTc	30	Yes	1.26 1.60	High specific activity colloid. (15mg/ml)
15	40	sulphur colloid	99mTc	30	Yes	1.18 1.81 (MMD)	Gravimetric analysis on cold (non-radioactive) sulphur colloid.
16	40	sulphur colloid	99mTc	30	Yes	1.38 1.81	Increased air flow through impactor by 10% to determine the effect of flow on particle size
17	40	sulphur colloid	99mTc	20	Yes	1.50 2.31	95-100% relative humidity to inlet air of nebulizer.

TABLE XIII (cont'd)

RUN #	MODEL	COMPOUND	LABEL	PRESSURE (PSI)	BAG-IN-BOX	AMAD (μm)	σ_g	COMMENTS
18	40	sulphur colloid	None	30	Yes	1.6 (MMD)	2.1	Al_2Cl_3 added to sulphur colloid preparation as an impurity (see text)
19	40	MAA	99 ^m Tc	30	Yes	1.2 (MMD)	4.1	Cold MAA used as solution (see text)
20	40	Aminex* exchange particles	99 ^m Tc	30	Yes	5	1.4	Very low output.
21	40	sulphur colloid	99 ^m Tc	30	Yes	1.07	1.56	Designed to determine the amount of particle trapping on an inline pneumotachometer.
22	40	sulphur colloid	99 ^m Tc	30	No	1.3	1.7	Direct connection between nebulizer & impactor, tubing length 35 cm., 0.005 gm's of gelatin added to 2 ml's of colloid.
23	40	sulphur colloid	99 ^m Tc	30	No	1.15 EST	1.7 EST	As above but 0.1 gm gelatin. Very low activity generated.
24	40	sulphur colloid	99 ^m Tc	20	No	1.74	1.75	As above but 0.2 gm of gelatin (maximum concentration)

TABLE XIII (cont'd)

RUN #	MODEL	COMPOUND	LABEL	PRESSURE (PSI)	BAG-IN-BOX	AMAD (µm)	σg	COMMENT
25	40	sulphur colloid	99 ^m Tc	20	No	1.25	1.8	Direct connection between nebulizer and impactor, tubing length 15 cm.
26	40	sulphur colloid	99 ^m Tc	30	Yes	1.31	1.73	0.05 ml Albumin (HSA) added as stabilizer
27	40	sulphur colloid	99 ^m Tc	30	Yes	1.29	1.73	0.05 ml Albumin (HSA) added as stabilizer.
28	40	Coulter Particles	None	30	Yes	2.03 (MMD)	2.25	Gravimetric analysis.

* Aminex A-29 exchange particles, control # 20142, lot # 16668 (BIO-RAD Laboratories, Richmond Cal.)

APPENDIX 4 TABLE XIV

HORIZONTAL (X AXIS) PROFILE

THROUGH THE SUMMED AXIAL FRAMES OF THE PHANTOM

COL	COUNTS	COL	COUNTS	COL	COUNTS	COL	COUNTS
1	0	17	16955	33	14313	49	36
2	0	18	17963	34	14915	50	1
3	0	19	17844	35	15323	51	1
4	2	20	16954	36	15273	52	2
5	6	21	16309	37	15316	53	0
6	3	22	16058	38	15717	54	0
7	2	23	15647	39	16264	55	0
8	0	24	15289	40	16705	56	0
9	0	25	15395	41	16932	57	0
10	0	26	15358	42	17448	58	0
11	3	27	14930	43	18003	59	0
12	75	28	14436	44	17264	60	0
13	1292	29	14510	45	14170	61	0
14	5178	30	14885	46	9261	62	0
15	10312	31	14802	47	4219	63	0
16	14539	32	14343	48	832	64	0

TABLE XV

VERTICAL (Z AXIS) PROFILE

THROUGH THE SUMMED AXIAL FRAMES OF THE PHANTOM

COL	COUNTS	COL	COUNTS	COL	COUNTS	COL	COUNTS
1	0	17	11293	33	14385	49	315
2	0	18	15054	34	14686	50	80
3	0	19	16965	35	14972	51	20
4	0	20	16976	36	14770	52	3
5	0	21	16496	37	14767	53	3
6	0	22	16094	38	15430	54	4
7	0	23	15402	39	15960	55	2
8	0	24	14984	40	16191	56	0
9	0	25	15135	41	16641	57	0
10	0	26	15279	42	17432	58	0
11	0	27	14962	43	17927	59	0
12	0	28	14381	44	17021	60	0
13	5	29	14436	45	14172	61	0
14	209	30	14975	46	9698	62	0
15	2397	31	15055	47	5086	63	0
16	6546	32	14632	48	1767	64	0

TABLE XVI

VERTICAL (Y AXIS) PROFILE

THROUGH THE SUMMED CORONAL PLANES OF THE PHANTOM

ROW	COUNTS	ROW	COUNTS	ROW	COUNTS	ROW	COUNTS
1	10	17	9882	33	10801	49	9611
2	39	18	10119	34	10907	50	9912
3	76	19	10098	35	11021	51	10276
4	173	20	10566	36	10668	52	7860
5	605	21	10795	37	10768	53	4026
6	1961	22	10710	38	10885	54	1367
7	4413	23	11270	39	10886	55	420
8	6865	24	10929	40	10863	56	166
9	8529	25	10894	41	10530	57	59
10	8982	26	11112	42	10786	58	47
11	8898	27	10981	43	10598	59	24
12	9174	28	11059	44	11146	60	3
13	9455	29	11019	45	10497	61	0
14	9714	30	11542	46	10356	62	0
15	10439	31	11192	47	10144	63	0
16	10324	32	11076	48	9850	64	0

APPENDIX 5 TABLE XVII

COUNT DENSITIES FROM THE ANTERIOR AND POSTERIOR
ROI LOCATED ON AXIAL PLANES OF THE PHANTOM

FRAME	ANT	POST	FRAME	ANT	POST
74	340	327	96	399	385
76	357	334	98	387	375
78	382	347	100	363	380
80	389	346	102	378	388
82	390	361	104	392	394
84	368	361	106	415	418
86	405	379	108	413	412
88	385	341	110	428	377
90	368	367	112	378	365
92	365	370	114	383	353
94	374	375			

APPENDIX 6 TABLE XVIII

PULMONARY FUNCTION DATA (% OF PREDICTED) FOR NORMAL SUBJECTS

SUBJECT	LUNG VOLUMES			AIRWAY FUNCTION				
	TLC (He)	FRC (He)	V _c	R _v (He)	FeV ₁ /V _c	\dot{V}_{50}	\dot{V}_{75}	DLCO(SB)
WL	111	143	113	113	79	102	67	136
PM	84	98	88	81	70	58	42	NA
DR	98	90	104	77	71	73	61	130
KH	98	138	96	119	74	59	41	112
MY	95	103	95	89	70	50	54	NA
HY	80	86	79	76	84	111	89	NA
DH	97	120	94	103	82	91	91	89
KM	100	127	96	114	89	115	108	NA
LO	108	137	105	115	84	100	71	110
DJ	113	135	118	96	81	59	79	131
JH	112	142	113	122	73	53	42	93
CM	129	131	138	97	67	58	62	119
CC	100	111	102	88	80	72	62	98

APPENDIX 7 TABLE XIX

VERTICAL PROFILES TAKEN THROUGH STATIC, SITTING,
 ANTERIOR AND POSTERIOR VIEWS OF THE RIGHT LUNG AFTER
 AEROSOL INHALATION ON SUBJECT JH

ANTERIOR

ROW	COUNTS	ROW	COUNTS	ROW	COUNTS	ROW	COUNTS
1	0	17	399	33	1949	49	1311
2	0	18	587	34	2079	50	1425
3	0	19	941	35	2129	51	1268
4	13	20	1371	36	2178	52	1065
5	14	21	1771	37	1982	53	802
6	22	22	2092	38	2041	54	655
7	26	23	2262	39	2038	55	393
8	35	24	2430	40	1933	56	318
9	46	25	2449	41	1785	57	209
10	30	26	2396	42	1891	58	127
11	58	27	2353	43	1772	59	44
12	81	28	2336	44	1764	60	3
13	112	29	2207	45	1627	61	0
14	120	30	2210	46	1633	62	0
15	142	31	2174	47	1614	63	0
16	214	32	2173	48	1482	64	0

POSTERIOR

ROW	COUNTS	ROW	COUNTS	ROW	COUNTS	ROW	COUNTS
1	0	17	440	33	2739	49	1153
2	0	18	665	34	2686	50	1104
3	1	19	949	35	2629	51	1037
4	3	20	1133	36	2545	52	892
5	12	21	1455	37	2693	53	703
6	18	22	1866	38	2387	54	555
7	9	23	2106	39	2415	55	435
8	24	24	2490	40	2107	56	320
9	22	25	2651	41	2044	57	195
10	31	26	2920	42	2026	58	144
11	45	27	2969	43	1884	59	67
12	87	28	3029	44	1756	60	14
13	125	29	2841	45	1780	61	0
14	168	30	2758	46	1652	62	0
15	239	31	2759	47	1423	63	0
16	307	32	2847	48	1373	64	1